Fall 12-16-2022

Anthropogenic Effects on Tidal Distortion in a Tidal River

Matthew D. Fischer
University of Maine, matthew.d.fischer@maine.edu

Recommended Citation

Fischer, Matthew D., "Anthropogenic Effects on Tidal Distortion in a Tidal River" (2022). *Electronic Theses and Dissertations*. 3727.
https://digitalcommons.library.umaine.edu/etd/3727

ANTHROPOGENIC EFFECTS ON TIDAL DISTORTION IN A TIDAL RIVER

By

Matthew Fischer

B.S. University of Alaska, Anchorage

A THESIS

Submitted in Partial Fulfillment of the

Requirements for the Degree of

Master of Science

(in Civil and Environmental Engineering)

The Graduate School

The University of Maine

December 2022

Advisory Committee:

Kimberly Huguenard, Assistant Professor of Civil and Environmental Engineering, Advisor

Lauren Ross, Assistant Professor of Civil and Environmental Engineering

Kelly Cole, Assistant Research Professor of Civil and Environmental Engineering

ANTHROPOGENIC EFFECTS ON TIDAL DISTORTION IN A TIDAL RIVER

By Matthew Fischer

Thesis Advisor: Dr. Kimberly Huguenard

An Abstract of the Thesis Presented
in Partial Fulfillment of the Requirements for the
Degree of Master of Science
(in Civil and Environmental Engineering)

Tidal rivers are landward portions of estuarine systems constituting the union between coastal, tidally controlled settings and rivers, where fluvial processes dominate. In these reaches, river discharge (mean flow) and tides are the two most important mechanisms in controlling geophysical flows. The processes governing water levels and current amplitudes in tidal rivers are highly nonlinear and modulated by external forcings- thus requiring sophisticated techniques for accurate prediction and forecasting. Physical oceanographers and estuarine physicists tend to limit their study area to the maximum extent of the horizontal tide (salinity intrusion), not the most landward point influenced by tidal water levels. This is in part because landward reaches are complicated by freshwater tributary inputs, tidal reflection, abrupt hydrographic changes, and backwater dynamics. Understanding river-tide interaction in tidal rivers is important for geomorphology as this synergism impacts salinity intrusion, sediment transport, pollutant fate, channel bifurcation, and deltaic deposition.

This thesis aims to satisfy two objectives: (1) to characterize the Penobscot River Estuarine (PRE) system and present field measurements collected in the tidal river section near the extent of salinity intrusion; and (2) to demonstrate the mechanism creating unexpected overtide patterns near the flood limit.

To accomplish these objectives, long-term water levels, meteorological, and river discharge datasets are used in conjunction with measurements collected during a field campaign conducted on September 21st, 2021. The results of this research effort reveal the modulations of the D2 tidal species with respect to mean flow and the emergence of hydrographic tidal reflection as a mechanism for generation of D6. The discussion presents a theory explaining momentum transfer to the D6 band under high mean flow conditions, where contributions from quadratic friction are known to decrease. This has implications in sediment transport, backwater dynamics, and longitudinal shifts of river-tide dynamics.

ACKNOWLEDGEMENTS

I would like to acknowledge and thank my research advisor, Dr. Kimberly Huguenard for allowing me this opportunity and mentoring me for the past two years. Thank you as well to Dr. Lauren Ross for your positivity and all you have taught me. A special thank you goes out to my fellow coastal graduate students, notably Lizzy, Sam, Reilley, and Liam for all your help and friendship, I could not have done it without you. Finally, I am grateful for my parents Tony and Melissa, and their encouragement throughout my academic career.

TABLE OF CONTENTS

LIST OF TABLES

LIST OF FIGURES

CHAPTER 1

INTRODUCTION

Of the various causes of change in water levels and currents in coastal environments, predictable astronomical tides are usually the most dominant. Tides are often referred to when talking about changes in water level, taking responsibility for dynamic balances between external forces such as atmospheric pressure, river flow, and density gradients acting upon coastal seas. This chapter introduces background information on surface gravity tides in coastal environments, as the ensuing chapters build on and integrate the shallow-water hydrodynamics of bays, estuaries, and rivers to study the resulting water levels and currents.

1.1 Tides

Tides are periodic fluctuations in water level, caused by the change of position of the Moon and Sun relative to that of the Earth (Case, 1999; Fry, 1987; Parker, 2007). The importance of tides has not gone unrecognized in the study of oceanography and estuarine science, as tidal currents and water levels affect mixing, stratification, and navigation. For its practical implications in currents and sea levels, tidal prediction is perceived to be one of the earliest topics studied in oceanography (Parker, 2007). The earliest known record of a tidal table originates in China in 1056 A.D. for the Tsientang River, as ancient seafaring civilizations first recognized its usefulness for navigation (Case, 1999).

Tides are surface gravity waves with long periods on the order of hours and days generated by gravitational attraction forces of the Sun and Moon and inertial forces constraining the dynamic systems in revolution about a common point, or barycenter (Parker, 2007). While the Earth and the Moon both revolve around their system's barycenter, a dynamic balance is found between gravitational attraction keeping the celestial bodies in contact, and centrifugal forces exerting an outward push keeping the bodies from spiraling inward into one another. As the Earth rotates on its axis, and the Moon orbits it in an elliptical path, gravitational attraction experienced at a particular location on the surface of the Earth constantly changes. The part of the Earth's surface closest to the Moon perceives greater gravitational attraction than centrifugal force, as gravity's influence is a function of distance, inversely proportional to the square of its distance. Conversely, on the opposite side of the Earth centrifugal forces overpower the Moon's gravitational attraction. These imbalances are still much weaker than Earth's gravitational field, pulling inward toward the Earth's core. Therefore, the substantive tide-producing forces are the vertical components of the moon's gravitational pull, acting tangential to the Earth's surface. Negligible forces oppose these, and the result is the movement of water in the ocean, contriving the tides. North or south of the equator, increasing or decreasing from zero in latitude, tides increase in amplitude because of the increased angle the location makes with the Earth-Moon system, similarly increasing the vertical component of the force (Fig. 1).

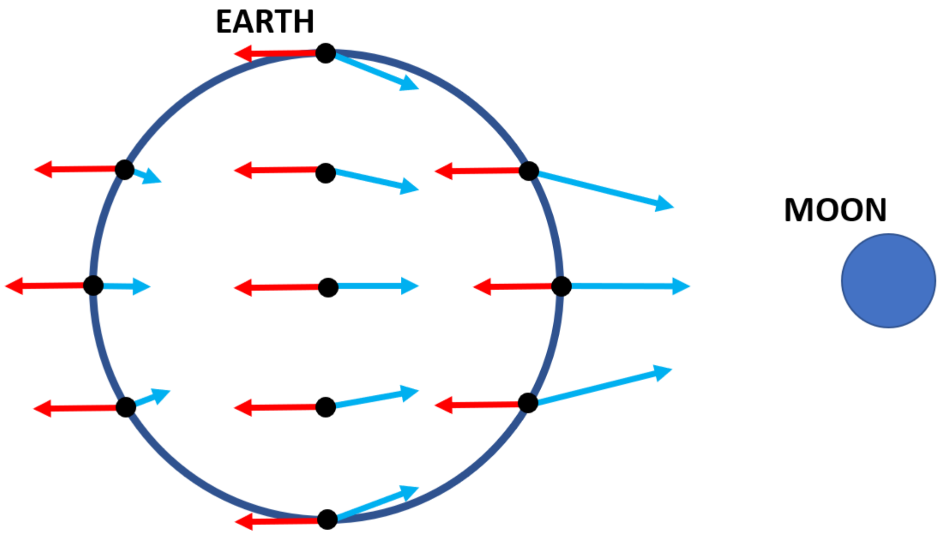

Figure 1: Tide-producing forces represented in 2D. The equilibrium theory of tides postulates that an oblate spheroid of water covers the earth, with twin, opposite, tidal bulges.

Tides typically have periods of multiple hours and wavelengths of hundreds to thousands of kilometers. Tidal ranges at a given location, the difference in elevation between consecutive high and low tides, depend on several factors. The primary factor in variable tidal range at a given location on the Earth's surface stems from the Sun and Moon's ever-changing position relative to the Earth. Periods exist where the bodies' gravitational fields act together, called syzygy. At this point in the orbital phases, the gravitational attraction from both celestial bodies acts along a common line, and constructive interference produces the greatest tidal range. This occurrence is commonly called a spring tide and is simply identified by the lunar phase, corresponding to new or full moons. Conversely, at the first and third-quarter points of the lunar phase, the two celestial bodies act at quadrature, or right angles to each other, producing a counteracting effect minimizing the tidal range, called neap tides.

Secondarily, parallax effects contribute to tidal range variation. The elliptical lunar orbit has a difference in minor and major axis distance from the earth varying by 50,000 km. This difference requires that the strength of the tractive force likewise vary through the lunar synodic period. When the Moon is closest to the earth, at perigee, tides are greater in amplitude. During apogee, when the Moon is at the furthest point in its orbit, tidal ranges decrease. The very same principle produces tidal variations for Earth's position in solar orbit. This tidal modulation is perihelion and aphelion, wherein the Earth is at its closest and furthest points from the sun.

Due to the vast difference in distances between the Sun and Moon with respect to Earth, the tide-producing force exerted by the Moon is roughly 2.5 times greater than that of the Sun. Regionally the tidal waveform differs because the sea level is heavily influenced by coastal topography. These differences become categorized into three distinct tidal regimes (Fig 2). In most places on Earth, the tidal regime is semidiurnal, marked by two highs and lows per day.

Diurnal tidal regimes are less prevalent but exist in a few places including the Gulf of Mexico and the Yukon-Kuskokwim Delta of western Alaska, possessing just one high and one low per day. Lastly, mixed semidiurnal tides encompass everything in between, characterized by two differing highs and lows per day.

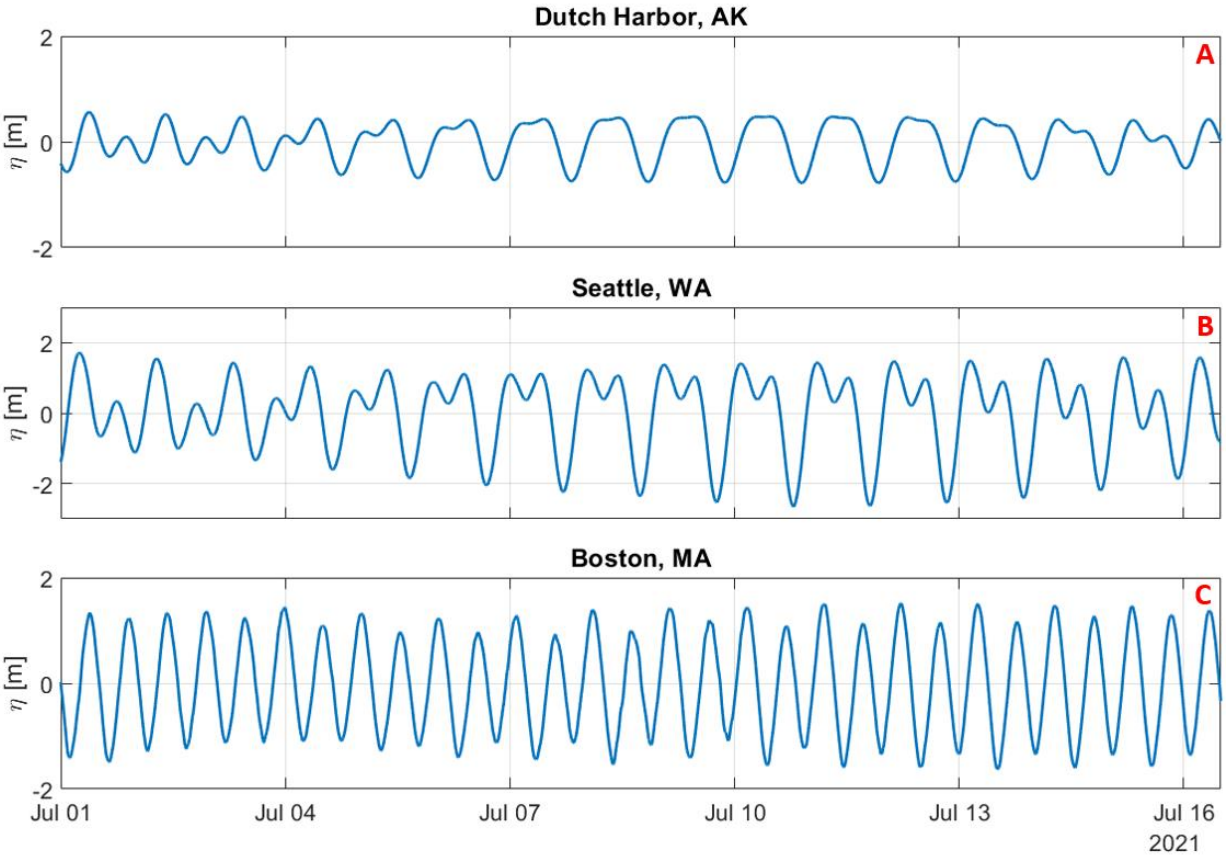

Figure 2: Tidal records from three different stations around the world showing remarkably different tidal signals over the first half of July 2021. Diurnal tides dominate Dutch Harbor, AK (A), Seattle, WA (B) is characterized by a mixed tidal regime, and Boston, MA (C) exhibits a semidiurnal tidal regime.

Specific contributions to the water level (tide) at a given location are tidal harmonic constituents, determined by deconstructing the total deviance from mean sea level into individual tidal components. Tidal harmonic constituents are simply frequencies at which the tide has energy. Each constituent is modeled as a wave, possessing an amplitude and epoch (phase lag), and its existence makes an independent contribution to the overall tide. Amplitude is the maximum height of the tidal constituent, and epoch is the time relative to some reference that this maxima contribution occurs. Astronomical constituents are named with a capital letter followed by a numeric subscript indicating the approximate number of cycles per day it makes. The main lunar harmonic constituent is M2, and the main solar is S2. The previously mentioned effects of non-circular and out-of-plane orbits in the Earth-Moon system are similarly represented by harmonic constituents. N2 represents the elliptical lunar orbit, and K1 and O1 express the effect of lunar declination. The sum of all these constituents, mathematically represented by cosine functions, reconstitutes the tide.

The act of decomposing a water level record into component constituents for a given location is tidal harmonic analysis. Pierre Simon Marquis Laplace was the first to suggest representing the tide as a sum of harmonic oscillations, but it was Lord Kelvin who developed the first theory of tidal harmonic analysis in 1868, recognizing the tides as a sum of periodic terms with amplitudes and phases. William Ferrel (1874) and George Darwin (1883) separately and simultaneously refined the harmonic method, both describing a useful harmonic method of tidal analysis and prediction in mathematical convention. Today sophisticated computer programs can decompose tidal records into constituents with immense accuracy through Fourier analysis and least squares techniques. In sum there are hundreds of tidal constituents, however accurate tidal prediction is possible with as little as twenty. The National Oceanic and Atmospheric Administration (NOAA) use thirty-seven that normally (as it differs by location) have the greatest effect on the water level in their tidal prediction scheme.

Conventional harmonic analysis does have limitations. The most important consideration affecting the accuracy of calculated harmonic constituents is the length of the discrete time series analyzed. The longer the record is, the closer in frequency two tidal constituents can be and remain distinguished, identified as unique constituents. Incorrectly assigned tidal spectral energy occurs when the length of the time series is less than the synodic period of two constituents with neighboring frequencies. In addition, conventional harmonic analysis methods confront severe challenges in the study of nonstationary signals with a tidal component. External forcings resulting in nontidal perturbations of water level in tidal frequency bands can create “smearing effects on the tidal spectral lines by nontidal energy” (Matte, 2012). Tidal rivers are dynamic zones wherein the water level response, unlike offshore coastal areas, is not always dominated by astronomical forcing, and is prone to nonstationary tidal signals.

1.2 Tidal Asymmetry

The dynamics of barotropic tides are accepted as linear in the deep ocean, where tidal amplitudes are on the order of one meter, and insignificant when compared to water depth (Parker, 1991). Over continental shelves and coastal areas, tidal waveforms become progressively distorted, losing the idealistic sinusoidal shape they have in the open ocean. This initiates tidal asymmetry, referring to inequalities now present in the flood and ebb phases of the tide.

Distortions or asymmetries in the tidal waveform are described with the inclusion of higher and lower harmonics, sub-harmonic and super-harmonic tidal frequencies that derive their energy from the principal astronomical constituents and possess integer fractions or multiples of their periods (Parker, 1986; Wang, 1999; Friedrichs & Aubrey, 1994). Higher harmonics are referred to as overtides or shallow-water constituents and are a consequence of hydrodynamics arising from the physics of water in motion. Nonlinear interactions in shallowing water generate overtides as the tidal range becomes significant compared to the depth, instigating nonlinearities

(Talke & Jay, 2020). The nonlinear terms contributing to the formation of shallow-water constituents emerge from the classical equations of tidal motion in one dimension (Table 1). Where (η) is water surface elevation from mean sea level, (u) is cross-sectionally averaged velocity, (h) is width averaged depth below mean sea level, (c_f) is a bed roughness coefficient equal to 0.0025, and (g) is the gravitational acceleration constant for the surface of the Earth (9.81 m/s^2).

Table 1: 1D Equations of Tidal Motion

$\frac{\partial u}{\partial t} + u\frac{\partial u}{\partial x} = -g\frac{\partial \eta}{\partial x} - c_f\frac{1}{h_0 + \eta}u\lvert u\rvert$	Eqn. 1.1 (Momentum)
$\frac{\partial \eta}{\partial t} + \frac{1}{b}\frac{\partial}{\partial x}[b(h_0 + \eta)u] = 0$	Eqn. 1.2 (Continuity)
$u\frac{\partial u}{\partial x}$	Eqn. 1.3 (*Advection*)
$\frac{\partial (u\eta)}{\partial x}$	Eqn. 1.4 (*Nonlinear Continuity*)
$c_f\frac{1}{h_0 + \eta}u\lvert u\rvert$	Eqn. 1.5 (*Bottom Friction*)
$\frac{u\lvert u\rvert}{h_0}$	Eqn. 1.5a (*Quadratic Friction*)
$\frac{\eta u\lvert u\rvert}{h_0^2}$	Eqn. 1.5b (*Depth Variation*)

Nonlinearity enters the mathematical representation of tides through the divergence of excess volume in the continuity equation and the advection and bottom friction terms in the momentum equation (Speer and Aubrey, 1985; Parker, 1984, 1991; Wang et al. 1999, 2002). The nonlinear terms in the equations of tidal motion are not tied to a single specific key parameter such as elevation or velocity, rather key parameters multiply one another, leading to energy transfer (Parker, 2007). The amplification and phase change of overtides depends on the energy transfer to them through nonlinear mechanisms. The sources of nonlinearity in the governing equations are *advection*, *nonlinear continuity*, and *bottom friction*. Equations 1.3 & 1.4 are classically the "shallow-water" terms. Equation 1.3 is the inertial term in the momentum equation, which represents the advection of momentum in the flow. Equation 1.4 is *nonlinear continuity* which accounts for nonlinearity in wave propagation velocity. Deep water tidal wave propagation velocity is approximately constant over an entire wavelength because depth is much greater than tidal amplitude $(\eta/h >> 1)$. In shallowing coastal environments, this does not hold as the crest travels faster than the trough, necessitating the *nonlinear continuity* term. *Bottom friction*, mathematically described by a nonlinear friction function (Eqn. 1.5), results in greater frictional damping in shallow water, slowing the propagation of tides at low water more than at high (Friedrichs & Aubrey, 1987; Dronkers, 1986). *Bottom friction* is further partitioned into *quadratic friction* and *depth variation* because of the two nonlinear aspects. The quadratic part ($u|u|$), and the elevation effect (η) (Parker, 2007; Godin & Martinez, 1994). *Quadratic friction*, presented in Equation 1.5a, contributes to the generation of odd harmonics (M6), and the loss of momentum from the main tidal constituent. Equation 1.5b gives *depth variation*, a relationship representing the effect of elevation on frictional momentum loss per unit volume of fluid. Fourier decomposition of the nonlinear terms reveals which frequencies receive tidal energy (Parker, 1984; Le Provost, 1991).

1.3 River-Tide Interaction

Tidal forcing is not the only phenomenon that modulates water levels and current amplitudes in estuaries. Nontidal forcing mechanisms such as wind, changes in atmospheric pressure, and variable river discharge contribute to nontidal changes in water levels that are aperiodic, unlike astronomical tides (Matte et al., 2012). Some forcings are affected seasonally and conform to annual variations, while other forcings such as local meteorological effects are comparatively short-lived. River-tide interaction generally refers to a frictional effect causing an exchange of spectral energy density between the tidal frequency band and the subtidal frequency bands (Sassi, 2013). Studies of river-tide interaction, specifically the effect of mean flow (river discharge) opposing tidal propagation have received research attention for the effects on the tidal range, vertical current structure, and spatial dissipation (Friedrichs, 2010; Cai et al., 2014; Dykstra et al., 2022; Elahi et al., 2020). Other preceding work in this vein has focused on implications related to sediment transport in highly nonlinear systems, backwater profiles in rivers with sloping beds, and the parametrization of bulk friction terms for increased ebb-cycle discharges (Fry, 1981; Kastner, 2019; Yoon, 2013). Previous studies demonstrated that the bi-directional flow of tidal currents and the unidirectional river discharge drive higher bulk friction during ebb cycles (Godin, 1985; Wu, 2021) from the currents acting in concert.

Mean flow distorts tides in tidal rivers by reducing the tidal range and transferring energy to higher frequencies (Parker, 1984; Dronkers, 1964; Gallagher & Munk, 1971). In tidal rivers subject to high mean flows, the processes that govern currents and water levels are highly nonlinear (Ippen & Harleman, 1966; Parker 2007; Dykstra, 2022; Friedrichs & Aubrey, 1988). These nonlinear interactions are therefore important in determining the tidal range, tidal current amplitudes, and timing of high & low waters. While the seaward discharge of the river is relatively low, the total height of the water column in the channel is similarly relatively low, resulting in increased bottom friction damping. This adds to the dissipation of tidal energy, reducing the tidal range, and reducing the spatial extent of the tidal intrusion. The balance of river discharge, frictional damping, and channel geomorphology determines whether tidal amplitudes decrease, remain constant, or increase along the length of the tidal channel. The ensuing chapter delves into the hydrodynamics throughout a tidal cycle and the intricacies of river-tide interaction in the Penobscot River Estuary.

CHAPTER 2

PENOBSCOT RIVER ESTUARY CHARACTERIZATION

2.1 Abstract

The Penobscot River Estuary (PRE) constitutes the junction of the Penobscot River, which drains 22,200 square kilometers of central Maine, and Penobscot Bay, a major inlet of the Gulf of Maine. The Penobscot River, originally named by the Indigenous peoples of the land, the Penobscot Nation, translates to “waters of descending ledge.” The University of Maine recognizes Marsh Island as the homeland of the Penobscot Nation, acknowledging the Penobscot Nation is a “distinct, sovereign, legal and political entity with its own powers of self-governance and self-determination and recognizes its place on Marsh Island in Penobscot Nation traditional territory” (UMaine MOU 2018). The objective of this chapter is to introduce the PRE, classify its estuarine characteristics, study the hydrodynamics through a complete tidal cycle, and present the dataset gathered and utilized in the ensuing chapter to delve into river-tide interaction in the PRE.

2.2 Introduction

The Penobscot River is New England’s second largest river system, flowing generally south, discharging into Penobscot Bay near Searsport, ME, where it joins the Gulf of Maine approximately 56 kilometers to the south. Four major tributaries feeding the Penobscot River are the West Branch Penobscot River, East Branch Penobscot River, Mattawamkeag River, and the Piscataquis River. In the nineteenth century, the Penobscot River was crucial to the world’s timber economy as a means of transportation. Bangor, ME was home to more than three hundred sawmills and the city bore the title of “lumber capital of the world” as demand for Maine’s white pines soared. Loggers would harvest, stockpile, and float timber downstream for refinement at sawmills in Bangor. Today the Penobscot River is recovering from contaminants such as sewage and industrial waste. Notably, mercury-containing chemicals, in which the dominant form is inorganic mercury (Geyer & Ralston, 2018). The largest contributor is suspected to have been the numerous sawmills that lined the banks, however, other point sources including a waste incinerator and Chlor-alkali production facility have been identified (Amirbahman & Merritt, 2008). Long recovery timescales were identified by a 2018 study conducted by Geyer & Ralston in the lower Penobscot River because the mechanisms that control the fate of contaminated sediments are bi-directional, translating downriver out estuary under periods of high discharge, and back up-estuary from tidal forcing under low discharge conditions. Estuarine settings such as the lower Penobscot tend to trap sediment and contaminants due to the convergence of flow associated with estuarine circulation.

2.3 Field Sampling

A field campaign conducted on September 21st, 2021, collected velocity profiles and micro structure in the channelized, tidal river portion of the PRE just south of Bangor to characterize the intratidal dynamics. Current velocities were measured with a Teledyne 1200 kHz RDI Workhorse Sentinel Acoustic Doppler Current Profiler (ADCP), transecting cross-river transects at two locations every hour for 13 hours (Fig. 3). The ADCP was towed downward facing on a trimaran, sampling at 600 Hz with bin sizes of 1m (horizontal) by 0.25m (vertical). The magnetic declination set for GPS (longitude & latitude) positioning function was set to 15.65^o for Hampden, ME. The widths of the North and South transects were 0.24km and 0.32km respectively, and channel depths ranged from 7.8-12.4m at the North transect and 5.7-10.8m at the South through the tidal cycle. The bathymetry of both transects was generally parabolic in profile, however, the North transect was more channelized and featured steeper banks. In addition to velocity measurements at each transect, vertical microstructure profiles were collected in the middle of the channel with a Rockland Scientific MicroCTD (conductivity, temperature, depth). Microstructure profiling was executed in an upward-profiling mode. The instrument was sunk with a weight and upon triggering the release mechanism, the instrument floated to the surface. The MicroCTD was equipped with two shear probes sampling at 512 Hz, JAC Fluorometer and JAC Turbidity sensors, and a high-resolution pressure sensor sampling at 64 Hz. Profiles where lines were tangled or exceeding a maximum angle of instrument inclination (10^{o}) were omitted. Profiles were collected in a burst of four to account for intermittency in turbulence, and the instrument ascended at an average rate of 0.6 m/s. The 4 profiles were interpolated onto a uniform vertical grid of 1m bins and averaged to provide one statistically significant profile for every hour. The rate of dissipation of turbulent kinetic energy (TKE), ε was calculated directly by integrating the velocity shear spectrum obtained via the two shear probes. Processing was conducted through the use of a Nasmyth spectrum following (Lueck et. al 2002; Bears, 2018). Assuming isotropic turbulence, the rate of dissipation of TKE can be described by (Eqn. 2.1), where ν is the kinematic viscosity of the fluid, k is the wavenumber, Ψ is the shear spectrum (Eqn. 2.2), and x is equal to $k\eta$ or $k(\nu^3/\epsilon)^{1/4}$, where η is the Kolmogorov microscale.

$$\varepsilon = \frac{15}{2}\nu \int_0^\infty \Psi(k)dk \qquad \text{Eqn. 2.1 (TKE)}$$

$$\Psi = \frac{8.05\mathrm{x}^{1/3}}{1+(20.6\mathrm{x})^{3.715}} \qquad \text{Eqn. 2.2 (Shear Spectrum)}$$

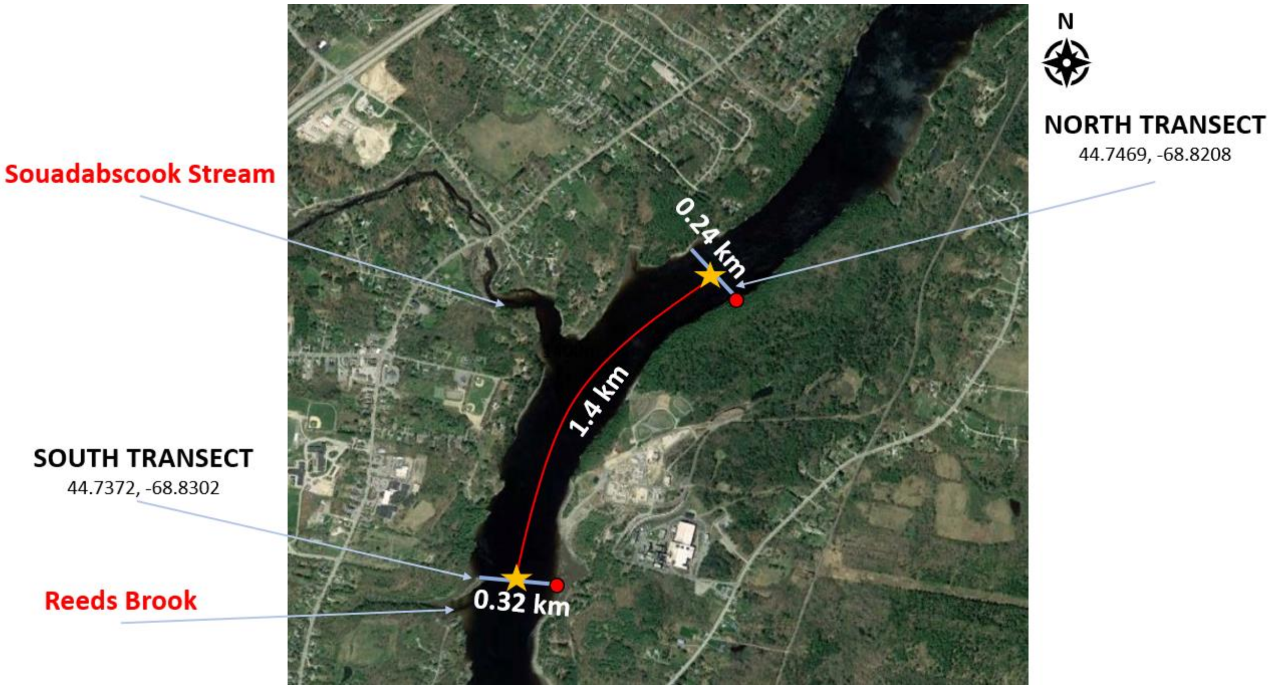

Figure 3: Aerial imagery of the sampling site in the Penobscot River with named tributaries. Locations of ADCP transect origins (red circles), and transects (blue lines) are included. MicroCTD profiling was conducted mid-transect and is designated by gold stars.

2.4 Results

The day of sampling on September 21st, 2021, was mostly clear and the precipitation total for the day was zero. The rate of discharge of the Penobscot River measured at the West Enfield USGS station was 191 m^3/s at the beginning of the day and 173 m^3/s by the end, as the contributing watersheds rate of emptying decelerated following a significant storm event on September 10th and 11th that brought about a peak discharge of 396 m^3/s. Wind speed and air temperature followed similar trends throughout the day reaching a maximum temperature of 21 $°C$ and maximum sustained 2-minute wind speed of 7 m/s from the south at approximately 3 PM (Fig.4). The study area did not experience any significant changes in atmospheric pressure, and winds were generally out of the southwest.

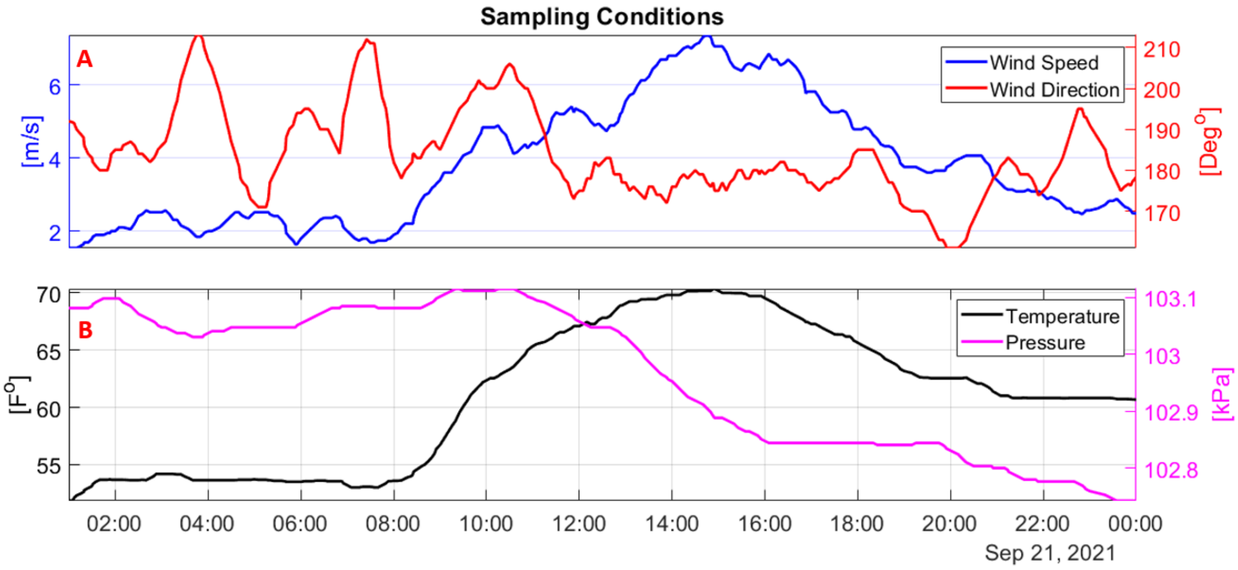

Figure 4: Environmental conditions displayed over the 9/21/21 day of sampling with (A) wind speed and direction, and (B) temperature & pressure.

Discharge of the Penobscot River cycles yearly, with spring freshets in April and May spiking the discharge curve to the yearly maxima (Fig. 5). The following summer months of June, July, August, and September constitute the dry, low flow periods where discharge is generally constrained below the 200 m^3/s threshold. Maximum discharges occur in the spring because of the additional contribution of snowmelt. The summer months are the driest and correspond to the smallest rates of river discharge. Sudden drastic increases in the discharge curve in October and November occur because of intense storms bringing heavy precipitation. Dataset maximum and minimum discharges of the Penobscot River are 2400 m^3/s and 50 m^3/s, respectively.

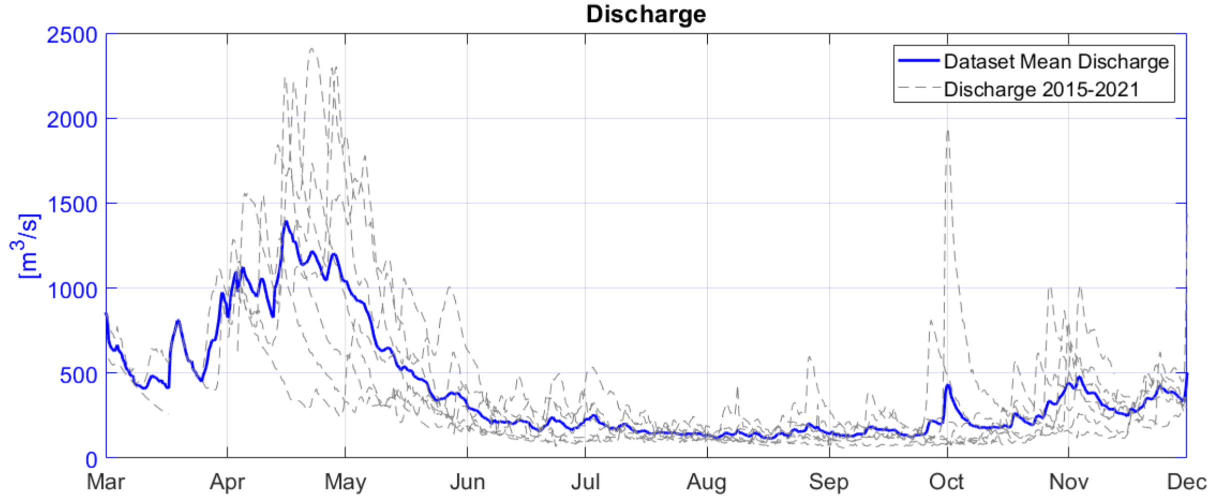

Figure 5: Penobscot River discharge collected from USGS station 01034500 at West Enfield, ME. Yearly discharges are plotted in dashed grey, and a 7-year annual mean is depicted in blue.

The Penobscot River Estuary is a mesotidal, hypersynchronous, and partially mixed estuary. Tidal waves enter the PRE from the south in the broad Penobscot Bay and propagate north as the system shallows in width and depth, increasing tidal amplitude. Tidal ranges grow from approximately three meters in Rockland at the mouth, to four meters at the head in Bangor, not shown but quantified from tidal records. Incident tides experience significant changes in water depth and morphology while propagating up the PRE, enhancing the potential for overtide generation. In the Penobscot River north of Bangor, the distinct tidal signal rapidly attenuates, and solely larger flood tides are discernable at the river gauge at Eddington (Fig. 6). Even further north at the gauge in West Enfield, the shape of the water level curve closely mirrors that of discharge, signaling the location of the tidal limit, the spatial extent of the tide. The presence of small tidal fluctuations at Eddington indicates that the tide undergoes a dramatic transformation in the river between Bangor and Eddington. Relative tidal energy decreases quickly landward of the flood limit, where river energy dominates (Dalrymple & Choi, 2007; Dykstra, 2022). The primary modulations of propagating tides arise from friction (bed stress), change in basin shape (convergence & reflection), bed gradient, and subtidal flows (discharge). For the tide to sharply attenuate over the 6km between Bangor and Eddington, one or a combination of these factors must also sharply change.

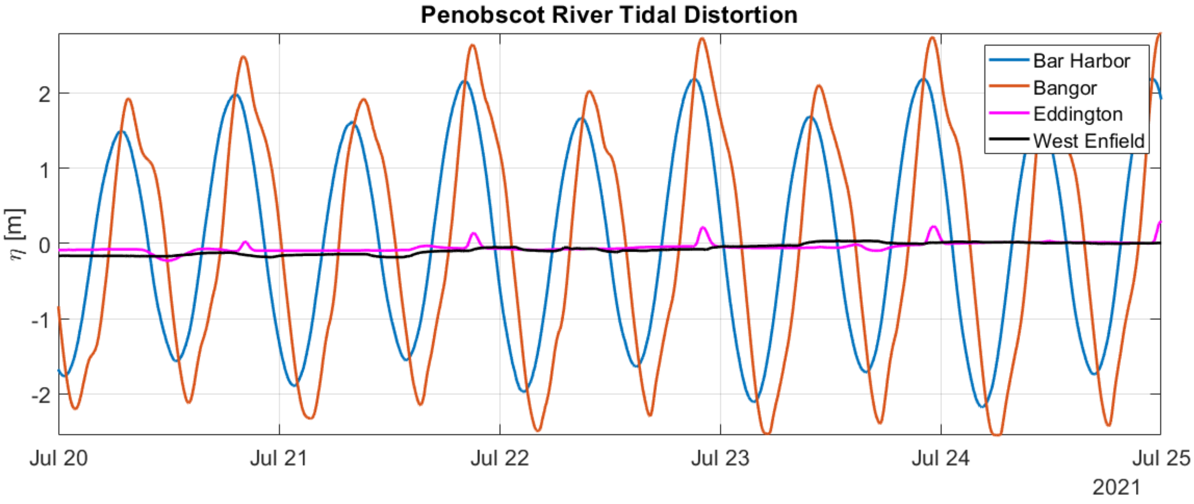

Figure 6: Evolution of demeaned water surface elevation along the PRE over 5 days in July 2021. The increase in tidal range and time lag (approximately 1 hour) between consecutive high and low waters is evident between Bar Harbor and Bangor. Larger flood tides are discernable at Eddington, displayed by small spikes in magenta. Tidal variation is not found in the black curve corresponding to West Eddington.

Harmonic analyses of water levels at Bar Harbor, serving as the coastal water level station at the mouth of the estuary reveals the tidal regime is semidiurnal, with the M2, N2, S2, and K1 constituents contributing the greatest to fluctuations in water level (Fig. 7). At the head in Bangor the constituents of greatest amplitude are M2, N2, S2, and M6. Constituent amplitudes show that in addition to the amplification discernable in the principal lunar & solar constituents, the emergence of overtides marks the water level record at Bangor. Diurnal constituents (D1) experience little amplification over the length of the estuary with a band amplitude increase of less than 5cm. The semidiurnal (D2) band has an aggregate increase of 0.29m, and sixth-diurnal (D6) band shows the greatest increase in spectral amplitude at 0.31m, followed by the quarter-diurnal (D4) band at 0.19m.

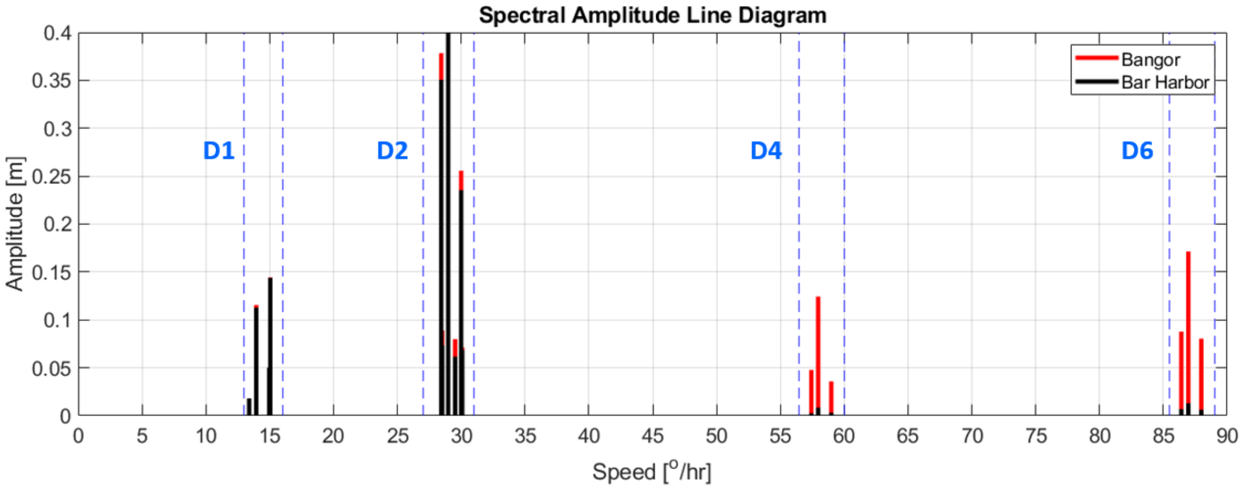

Figure 7: Spectral amplitude line diagram illustrating the amplification and emergence of overtides in the PRE. Amplitudes were derived from tidal harmonic analysis performed on water level records at Bangor & Bar Harbor. The principal lunar semidiurnal constituent (M2) is omitted from the figure to save the vertical scale, the M2 grows approximately 0.21m between the stations. Constituents included in the figure are K1, O1, P1, Q1, M2, N2, S2, K2, L2, NU2, M4, MN4, MS4, M6, 2MN6, 2MS6, the greatest contributors to water level for their respective bands. Black and red vertical lines give amplitude at Bar Harbor and Bangor, respectively. Dashed blue lines designate frequency bands, and the x-axis is given in units of degrees per hour.

The delineation between the coastal and river reaches of the PRE is clear as harmonic analysis methods indicate the coastal station in Bar Harbor lacks the environment for instigating shallow-water nonlinearities and generating a distorted tide. The increase in the D6 band at Bangor is remarkable, as generally, the D4 band is the dominant contributor to tidal distortion.

The emergence of D6 significance suggests that quadratic friction is the dominant nonlinear term, attributed to transforming energy to sixth-diurnal oscillations.

Channel velocity measurements detail bi-directional currents through the tidal cycle, signaling that the sampling location is seaward of the flood limit and within the extent of the horizontal tide (affected by tidal currents) of the PRE (Fig. 7). Maximum current velocities on ebb (-0.83 m/s) exceed that of flood (0.63 m/s) on the day of sampling because of additional downstream momentum from river discharge. The North transect experienced slightly greater flood velocities than the South transect because of additional width convergence, as the South transect is shallower, broader, and has more storage capacity. South transect ebb velocities are similar to the North, even with the additional downstream freshwater input of the Souadabscook stream tributary (Fig. 8). The evident tidal distortion discernable in curve of water level on the ebb phase is a result of the lessening of ebb velocities that occur approximately two hours before. The tidal river section of the PRE is flood dominant, characterized by longer falling tides, and stronger flood currents. Yearly average ebb-phase duration for 2021 was calculated to be 6.7 hours, obtained from a zero-crossing analysis performed on the water levels at Bangor (not shown). Shorter flood durations necessitate greater velocities to retain a volume equilibrium.

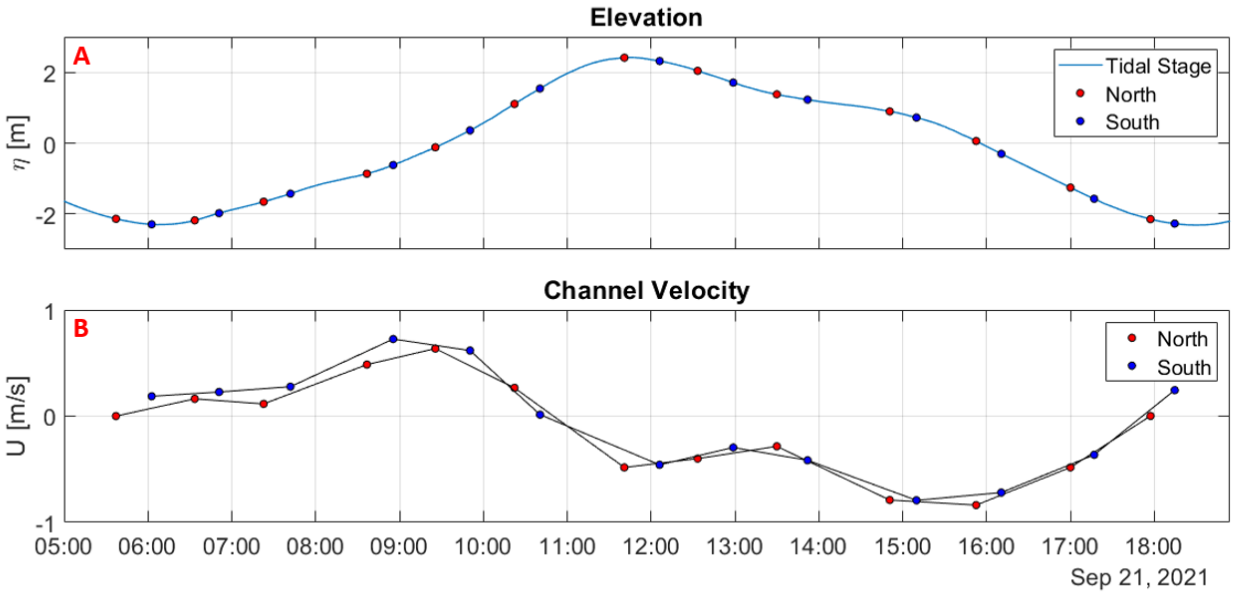

Figure 8: Elevation (A) and depth-averaged channel velocity (B) from the Bangor USGS station with red and blue filled circles designating the times of ADCP transecting. Current velocities are shown to lead elevation by approximately 2 hours.

Turbulence and conductivity measurements obtained mid-channel detail the oscillatory nature of characteristics of the fluid and flow through a tidal cycle. During the day of sampling, river discharge was relatively low (<200 m^3/s), which is less than half of the 7-year average, but still strong enough to restrain the limit of salinity intrusion downriver of the sampling location. This is apparent in the density and salinity measurements, showing a minimal influence of denser, saltier seawater at the end of the flood phase (Fig. 9). The water surface sees much less variation in tracers than at depth as the denser, saltier, and colder water is advected at depth and restrained to the bottom of the water column by vertical stratification. The time dependent salt-wedge character of the PRE restrains seawater with strong horizontal stratification. Temperature exhibits more vertical homogeneity on flood phases on the tide, as diffusion and advection work in concert to mix the fluid. Variations in the water column thermal structure are also discernable on a diurnal timescale. Dissipation peaks at 1.11e-05 m^2/s^3 (shown as -4.65 in the contour in the

$\log_{10}$ scale) just after slack water when flow switches direction, during the beginning of the flood phase.

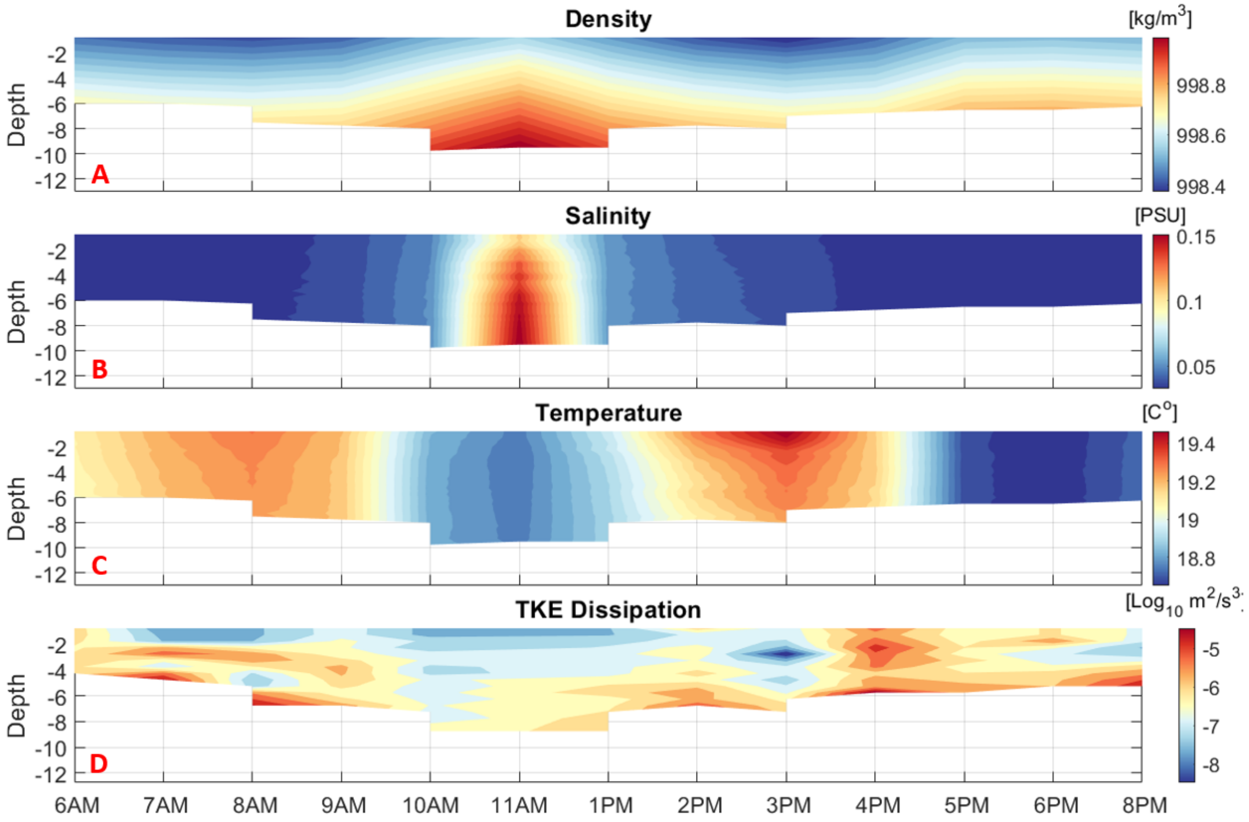

Figure 9: MicroCTD profiling output depicted through time with contour plots of (A) fluid density, (B) salinity, (C) temperature, and (D) dissipation. Density reaches a maximum at depth when saltier, denser water is advected upstream via incident tides. Temperature variation is also linked to the phases of the tide as the coastal water is colder. Dissipation in the channel reaches a maximum at approximately 4 PM on the ebb phase of the tide.

2.5 Discussion

Challenges emerge when categorizing estuaries because of the broad range of advanced estuarine dynamics that exist. In addition, geomorphic characteristics such as inlet geometry, sinuosity, convergence, and longitudinal length also add diversity to the breadth of systems. Estuaries have historically been classified by the characteristics of stratification and circulation. This method is limited by variability in those same characteristics, which may vary over an order of magnitude within the spring-neap cycle. Categorization by employing non-dimensional numbers that describe the estuaries principle forcing variables such as the freshwater Froude number (Fr_f) and a mixing parameter (M) is an alternative parameterization (Geyer & Macready, 2014) that is posited to effectively separate different estuarine regimes, and addresses key issues of initial vertical salinity difference, and effectiveness of vertical mixing.

$$Fr_f = \frac{U_R}{\sqrt{\beta g s_{ocean} H}} = 2$$ Eqn. 2.3 (Freshwater Froude Number)

$$M^2 = \frac{C_D U_T^2}{\omega N_0 H^2} = 1.1$$ Eqn. 2.4 (Mixing Parameter)

The Freshwater Froude Number describes net velocity due to river flow scaled by frontal propagation speed, and the mixing parameter quantifies the effectiveness of tidal mixing for a stratified estuary. U_R is discharge velocity, β = 7.7×10^{-4}, N_0 is the buoyancy frequency, equivalent to $(\beta g s_{ocean} H)^{1/2}$, s_{ocean} is the coastal water salinity, H is a characteristic depth, C_D is a drag coefficient in the range of $1 - 2.5 \times 10^{-3}$, U_T is the amplitude of depth-averaged tidal velocity, and ω is the tidal frequency. Under these criteria, the PRE is classified as a time-dependent salt wedge estuary, strongly forced by both tides and river flow. The general seasonal periodicity in these forcing mechanisms enables a large mass of contaminated sediment to redistribute over seasonal timescales (Geyer & Ralston, 2018). Bi-directional transport, the primary driver in balance between sediment trapping and remobilization, explains a long dilution time of 25 years identified for mercury contaminants in the PRE. The fate of these contaminants signals the PRE is a mature-leaning geomorphic system, with well established estuarine and fluvial environments.

2.6 Conclusion

A field campaign conducted in the Penobscot River Estuary near Hampden in September of 2021 provided velocity structures and turbulence profiles to elucidate the hydrodynamics through a tidal cycle. Intra-tidal variations in fluid density, salinity, and temperature are all dependent on tidal forcing and the up-estuary advection of seawater. Periodic distortions in tidal water levels attributed to overtides were identified at Bangor from harmonic analysis, with D6 band harmonics the dominant contributor to higher frequency fluctuations in water level. Seasonal periodicity was recognized in river discharge, with sustained increased river discharges ($>500 m^3/s$) occurring in the spring. Furthering the understanding of local tidal patterns, river discharge, and local meteorology is important background for the study of river-tide interaction. The need for additional studies in this environment is evident as still today the effects of previous malpractice are recognized in the Penobscot River Estuary.

CHAPTER 3

ANTHROPOGENIC EFFECTS ON TIDAL DISTORTION IN A TIDAL RIVER

3.1 Abstract

Tidal distortion induced by nonlinear interactions in shallow water evokes responses in water level, current amplitude, sediment transport, and tidally averaged mean sea level. Studies of river-tide interaction in tidal rivers, specifically in environments with engineered structures has received little attention. This work examines the effects of mean flow on tidal asymmetry-delving into the sources of generation for the D2 tidal species in the tidal river portion of the Penobscot River Estuary (PRE) and detailing the mechanisms responsible for generating a D6 that dominates the D4. Long-term time series of water levels were obtained from the confluence of the Penobscot River and Kenduskeag Stream in Bangor, ME to understand how mean flow modulates the quarter- and sixth-diurnal tidal species in an engineered (i.e., partial dam remnants, seawalls, bridges) section of the tidal river. In combination with this, in situ field observations were collected to quantify the nonlinear mechanisms dominating overtide generation. Cross-sections of current velocity were collected at two locations across the Penobscot River with a downward-facing Acoustic Doppler Current Profiler for a tidal cycle during low (<200 m^3/s) river discharge conditions. New findings explicate that tidal energy is transformed to D6 harmonics by morphologic tidal reflection via a nonlinear interaction with the principal tide. This result has consequences in compound flooding, tidal distortion, and sediment transport.

3.2 Introduction

In shallow coastal settings, estuaries provide a transitional pathway for tidal energy to propagate landward towards concentrated areas of infrastructure, economic centers, and human populations. The evolution of tidal energy, the primary driver of water motion in estuarine environments, has been studied extensively (Lamb, 1932; Ianniello, 1977). Landward regions of applicable estuaries are called tidal rivers, existing upstream of the maximum limit of salinity intrusion and downstream of the limit of the vertical tide (tidal fluctuations in water level) (Whitfield & Elliot, 2011). These channelized portions of estuaries are characterized by water levels and current amplitudes that are controlled by a dynamical balance between oceanic, meteorological, hydrologic, and climatic forces (Matte et al., 2013). Of greatest significance are the river and the sea forcings of freshwater discharge and incident tides. Such areas where the two forcings act can extend inland for hundreds of kilometers and are shaped geomorphologically by bi-directional flow (van Rijn, 2011). Tides in rivers can be represented as nonstationary signals and are highly variable, evolving over time, perturbed by abrupt, aperiodic, quasi-periodic, and secular forcings (Matte, 2013). The narrow, channelized nature of tidal rivers promotes higher mean flows from river discharge compared to their estuary counterparts, leading to enhanced tidal distortions through the development of overtides. In theory, it is expected that the quarter-diurnal overtide generally increases as mean flow increases, while the sixth-diurnal overtide decreases (Parker, 1991). At relatively small ratios of tidal current amplitude ($u_0/u_1 < 0.2$), the D6 band is greater than D4 because of weak river discharge and the resulting low amount of tidal energy transformed to D4. At ratios in the ($0.2 < u_0/u_1 < 1.0$) range, momentum transfer to D4 exceeds the diminishing D6. For ratios greater than 1 ($u_0/u_1 > 1.0$), river discharge overpowers tidal currents, flow is unidirectional, and momentum input to D6 ceases (Fig. 10).

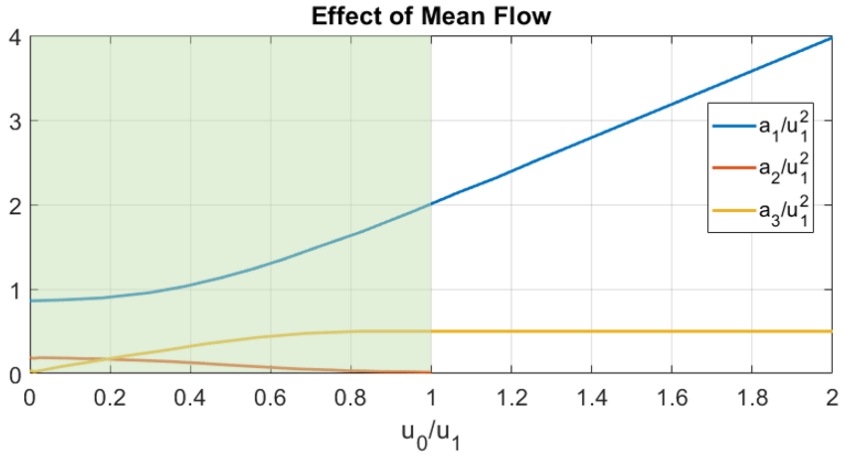

Figure 10: Effect of mean flow on the first three tidal harmonics from Fourier analysis of the quadratic friction term. Mean flow velocity is designated u_0, and u_1 is tidal current amplitude. a_1 is a friction coefficient tracking momentum loss from the main tidal constituent. a_2 and a_3 represent momentum input to second and third harmonics. The area shaded in green highlights conditions where D4 increases & D6 decreases. Adapted from Parker, 1991.

In the tidal river portion of the PRE, the sixth-diurnal overtide amplitude remains elevated despite high mean flows and often exceeds the quarter-diurnal overtide amplitude (Spicer, 2019). The effects of variable river discharge on longitudinal variation in tidal dynamics are poorly understood, as many previous studies have used relatively stable (nearly constant river discharge) or ideal estuaries. The goal of this work is to understand the relationship between the quarter- and sixth-diurnal overtides with the mean flow and principal tide. The research objectives are to characterize the tidal behavior in the tidal river portion of the PRE, to demonstrate the mechanism causing elevated D6 amplitudes during high river discharge periods, and to explain the evident deviation from theory.

The following work begins with a background into overtide theory and development, followed by a description of the PRE system. An outline of data collection, processing techniques used, and presentation of results follows. Seven years of water level data alongside in situ transecting measurements will show that the sixth-diurnal constituent dominates the overtides during high and low discharge periods. The discussion will explore the role of geomorphology and hard structures in enhancing tidal distortion. The conclusion section emphasizes the role of tidal reflection in tidal distortion and discusses potential implications for material transport and compound flooding.

3.3 Overtides

Periodic tidal asymmetry in the water level record can be described with the inclusion of higher and lower harmonics, tidal frequencies that derive energy from the principal astronomical constituents and possess integer fractions or multiples of their periods (Parker, 1986). Higher harmonics, referred to as overtides or shallow-water constituents, are a consequence of hydrodynamics, born out of the physics of water in motion. Generated by nonlinear interactions in shallowing water as the tidal range becomes no longer insignificant compared to tidally averaged depth (Talke & Jay, 2020). The amplification and phase change of overtides in a species depends on the energy transfer to them through various nonlinear mechanisms. In tidal rivers subject to high river discharges, the processes that govern currents and water levels are highly nonlinear (Ippen & Harleman, 1966; Friedrichs & Aubrey, 1988; Parker, 2007). These nonlinear interactions determine the tidal range, speed of tidal currents, timing of high & low waters, and tidal regime. Classical equations of tidal motion in one dimension and the nonlinear terms contributing to the formation of shallow-water constituents are:

$$\frac{\partial u}{\partial t} + u\frac{\partial u}{\partial x} = -g\frac{\partial \eta}{\partial x} - c_f\frac{1}{h_0 + \eta}u|u|$$ Eqn. 3.1 (Momentum)

$$\frac{\partial \eta}{\partial t} + \frac{1}{b}\frac{\partial}{\partial x}[b(h_0 + \eta)u] = 0$$ Eqn. 3.2 (Continuity)

$$u\frac{\partial u}{\partial x}$$ Eqn. 3.3 (*Advection*)

$$\frac{\partial(\mathrm{u}\eta)}{\partial \mathrm{x}}$$ Eqn. 3.4 (*Nonlinear Continuity*)

$$\mathrm{c_f}\frac{1}{\mathrm{h_0}+\eta}\mathrm{u}|\mathrm{u}|$$ Eqn. 3.5 (*Bottom Friction*)

$$\frac{\mathrm{u}|\mathrm{u}|}{\mathrm{h_0}}$$ Eqn. 3.5a (*Quadratic Friction*)

$$\frac{\eta\mathrm{u}|\mathrm{u}|}{\mathrm{h_0^2}}$$ Eqn. 3.5b (*Depth Variation*)

Where (η) is water surface elevation from mean sea level, (u) is cross-sectionally averaged velocity, (h) is width averaged depth below mean sea level, (c_f) is a bed roughness coefficient equal to 0.0025, and (g) is the gravitational acceleration constant for the surface of the Earth (9.81 m/s^2). Nonlinear terms in the equations of 1D tidal motion (Eqns. 3.1 & 3.2) are not tied to a single specific key parameter such as elevation or velocity, rather key parameters multiply one another, leading to energy transfer (Parker, 2007). The sources of nonlinearity in the governing equations of tidal motion are *advection*, *nonlinear continuity,* and *bottom friction*. Eqns. 3.3 & 3.4 are classically referred to as “shallow-water” terms. Eqn. 3.3 is the inertial term in the momentum equation, which represents the advection of momentum in the flow. Eqn. 3.4 is *nonlinear continuity* which accounts for nonlinearity in wave propagation velocity. Deep water wave propagation velocity is approximately constant over an entire wavelength because depth is much greater than tidal amplitude ($\eta/\mathrm{h} >> 1$). However, in shallow coastal settings, the crest travels faster than the trough. *Bottom friction*, mathematically described by a nonlinear friction function (Eqn. 3.5), results in greater frictional damping in shallow water, slowing the propagation of tides at low water more than at high (Dronkers, 1986; Friedrichs & Aubrey, 1987). *Bottom friction* is further partitioned into *quadratic friction* and *depth variatio*n because of the two nonlinear aspects, the quadratic part ($u|u|$), and the elevation effect (η) (Parker, 2007). *Quadratic friction*, presented in Eqn. 3.5a contributes to the generation of odd harmonics (D6), and the loss of momentum from the main tidal constituent. Eqn. 3.5b gives *depth variation*, a relationship representing the effect of elevation on frictional momentum loss per unit volume of fluid. A Fourier analysis of the nonlinear terms can reveal what frequencies receive tidal energy (Parker, 1984; Le Provost, 1991).

Channelized tidal rivers, such as the northern extent of the PRE, are strongly nonlinear systems forced predominantly by barotropic tides. As mean flow increases in the PRE, so does frictional momentum loss from the main tidal constituent, attenuating the incident tidal wave propagating up estuary, and decreasing the tidal range (Godin, 1999; Toffolon & Savenije, 2011). Mean flow distorts the tidal waveform by reducing the tidal range and transferring energy to higher frequencies (Dronkers, 1964; Gallagher & Munk, 1971; Parker, 1984). This dampening relationship is balanced by width convergence, amplifying tidal waves in hypersynchronous estuaries. Tidal range reductions lessen moving out estuary, as the velocity of mean flow decreases while the estuary widens. Generation of a second harmonic, D4 and increases in sea surface distortion (D4/D2) are a result of the two shallow-water terms, nonlinear frictional interaction of the mean (river) and tidal flow (principal tide), and the friction loss of momentum per unit volume of fluid, the so-called elevation effect (Parker, 1984). It follows that the D4 overtide is sensitive to variations in mean flow (Parker, 2007). A third harmonic, D6, is generated by the *quadratic friction* portion of the bottom friction term. As mean flow increases the generation of D6 decreases, until the ratio of mean flow to tidal current amplitude reaches unity ($u_o/u_1 = 1$) and the flow is unidirectional, and momentum input to D6 is zero (Parker, 2007). Typically, the D6 amplitude is <10% of the D2 amplitude when it appears (Parker 1991;

Blanton et al. 2002). The average D6 amplitude in the tidal river portion of the PRE, the location of the study site presented in the following section, is 14% of the average D2 amplitude.

3.4 Study Site

The PRE (Fig. 11) is an approximately 100-kilometer-long system, constituting the junction of the Penobscot River, draining 22,274 km2 of central Maine, and Penobscot Bay, a major inlet of the Gulf of Maine (Spicer, 2017). The Penobscot River is Maine's largest and New England's second-largest river system, flowing generally south, debouching into Penobscot Bay at Searsport, where it joins the Gulf of Maine approximately 56 km to the south (Geyer & Ralston 2018). The estuary extends 35 km seaward from the limit of tidal influence at the Veazie Dam near Bangor and acts as a tidally forced salt wedge under high discharge conditions (Geyer & Ralston 2018). The Penobscot River has an annual average discharge of approximately 350 m3/s, a peak annual discharge of approximately 1800 m3/s, and a flow minimum of approximately 150 m3/s. Salinity content in the PRE ranges from 0 to 30 PSU, and temperatures range from 0–20 °C through the annual cycle (Geyer, 2017). Width varies from 30 km at the mouth, converging to 0.24 km at the head at Bangor, where tidally averaged depth also diminishes to 5.5 m (Spicer, 2019). The PRE is a hypersynchronous, midlatitude estuary, seasonally affected by ice cover, acting to dampen the tidal range (Georgas, 2012). Isolated storm events such as cyclonic vortices in the Western Atlantic induce low-frequency storm surges in the PRE, accompanied by high winds and heavy precipitation. The amplitude of storm surge at Bangor can be twice that at the estuary mouth, a consequence of tide-surge-river interaction. Under significant storm surge conditions, tide-surge interaction can produce D6 & D8 oscillations with larger amplitudes than the principal tidal component (D2), owed to quadratic friction and resonance mechanisms respectively (Spicer, 2019).

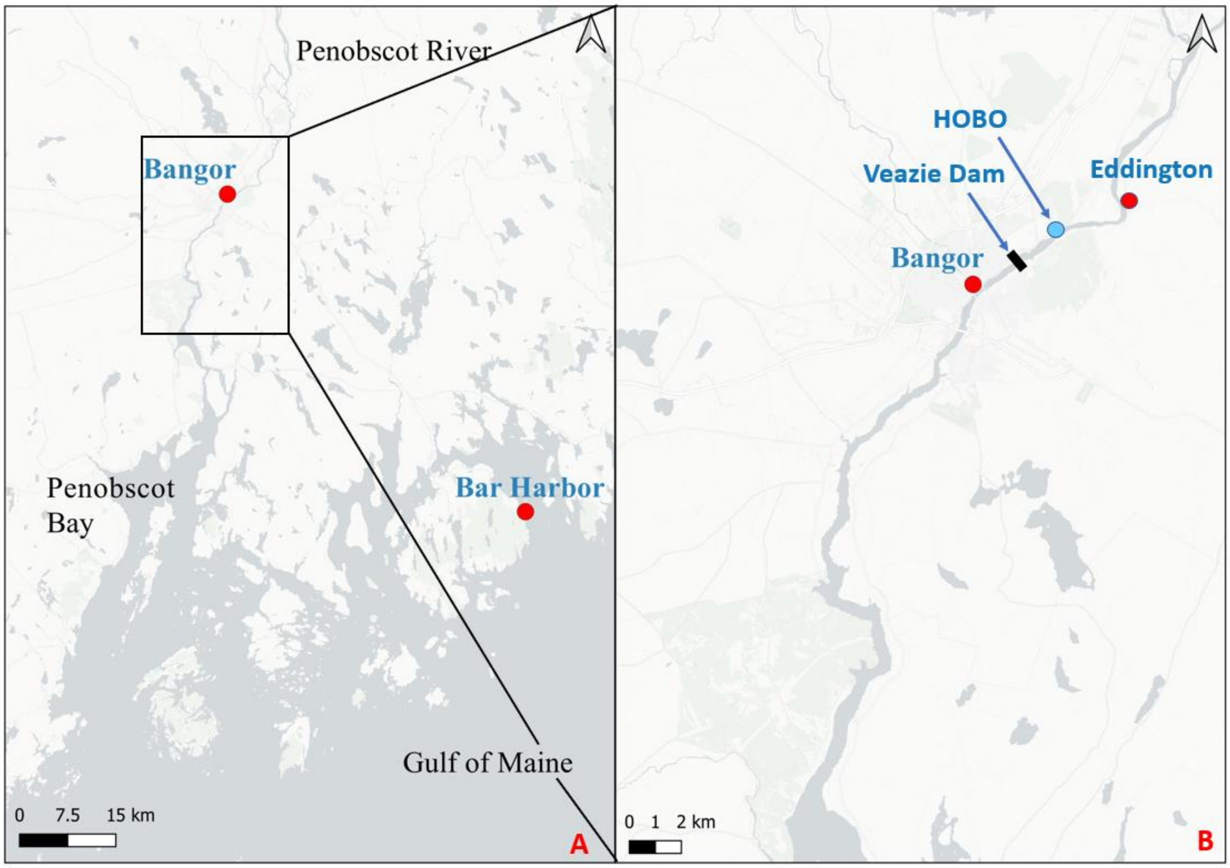

Figure 11: Aerial site map depicting the PRE and major bodies of water (A) and a tighter view of the tidal river portion of the PRE proximate to Bangor (B). Red circles designate the locations of NOAA/USGS stations, the blue circle marks the location of a deployed pressure sensor, and the black rectangle marks the location of the Veazie Dam.

3.5 Data Collection

The primary observations used in this study are water level and discharge records provided by the National Oceanic and Atmospheric Administration (NOAA), and the U.S. Geological Survey (USGS), respectively. Stations at Bangor (USGS 01037050), Eddington (USGS 01036390), and West Enfield (USGS 01034500) constituted the long-term river monitoring data used. USGS stations sample water level and discharge at 15-minute and 6-minute intervals (2015-current) and are collectively referenced to the North American Datum of

1983 (NAD83). River discharge data gathered from West Enfield is approximately 55 km upriver of Bangor and 80 km from the head of Penobscot Bay. Meteorological data, including wind speed and direction at 10 m elevation made available by the MesoWest project, an active open-source archive of weather observations across the United States. Specific to this project is Station KBGR at the Bangor International Airport, approximately 4.8 km from the study site in the Penobscot River. A NOAA buoy at Bar Harbor (NOAA 8413320) supplied coastal water level records in the Gulf of Maine. Additionally, an ONSET HOBO water level data logger (U20L-02) was deployed from the bank of the Penobscot River throughout November 10-29th, 2021 to collect water level measurements at the confluence of the Penjajawoc Stream and the Penobscot River, between Bangor and Eddington, north of the Veazie Dam. The HOBO logger continuously sampled absolute pressure and temperature at a 2-minute interval throughout the deployment period.

A field campaign conducted on September 21st, 2021, collected velocity profiles in the channelized, tidal river portion of the PRE just south of Bangor in Hampden, ME in order to characterize the intratidal dynamics. Current velocities were collected with a Teledyne RDI 1200 kHz Workhorse Sentinel Acoustic Doppler Current Profiler (ADCP), transecting cross-river at two locations every hour for 13-hrs. The points of origin for the north and south ADCP transects were (44.74688°, -68.82081°) and (44.73710°, -68.83019°) respectively (Fig. 12).

Figure 12: Penobscot River sampling site aerial with named tributaries. Locations of cross-channel ADCP origins (red circles) and transects (blue lines) are overlaid. Cross-channel distances and along-channel distance between the North and South transects are given in white.

3.6 Data Processing

Water levels from NOAA (Bar Harbor) and USGS (Bangor, Eddington, West Enfield) stations were linearly interpolated onto uniform 6-minute interval time vectors. The minimum resolution of the water level dataset was 15-minute sampling at the USGS gauge in Bangor in 2015 and part of 2016. Frequency spectrums of yearly, ice-free water level data at Bangor and HOBO pressure sensor data were obtained with Welch's power spectral density (PSD) estimate, segmented into eight periodograms using a 50% overlapping Hamming window. Confidence intervals (95%) given for the spectra were calculated via a chi-square inverse cumulative distribution function. Nonstationary analysis of tidal records was conducted via wavelet transforms, decomposing the time series into time-frequency space with a continuous wavelet transform (CWT), adhering to the discrete notation and details presented by Torrence & Compo, 1998.

$$W_n(s) \; = \sum_{n\prime\,=\,0}^{N-1} x_{n'} \psi * \left[\frac{(n' - n)\delta t}{s}\right] \qquad \text{Eqn. 3.6 (Continuous Wavelet Transform)}$$

Where W_n is the continuous wavelet transform of the discrete time series, x_n. Wavelet scale is given by s, n represents the localized time index, N is the length of the time series, and ψ is the chosen basic function. Transforms were performed with Morlet basis functions ($\psi_0(\eta) = \pi^{-1/4} e^{i\omega_0 \eta} e^{-\eta^2/2}$) and a cone of influence (COI) for delineating statistical significance, necessary because padding with zeros will reduce amplitudes near the edges at larger scales. The region of the wavelet spectrum falling outside the COI, defined by the e-folding time for each scale ($\tau_s = \sqrt{2}s$), is disregarded as edge effects introducing discontinuities become important. Tidal bands of interest were reconstructed with the real part ($\Re\,\{W_n(s)\}$) of the wavelet transform (Eqn. 3.6) and a zero-crossing method extracted crests in the waveforms to serve as band amplitude. The frequency band limits for reconstructions of D2, D4, and D6 were 12.2-12.6, 6.1-6.4, and 4.0-4.3 hours, respectively.

Velocity measurements were collected with the ADCP, and after removing bad ensembles, were binned onto 1m x 0.25m grids and rotated to principal along and cross-channel components via principal component analysis. The middle 20% of the river was laterally averaged to provide a single measurement at each vertical bin for the flow velocity of the channel. HOBO pressure sensor data was converted to water column depth with compensation for the effects of barometric pressure and temperature. Atmospheric pressure used in the conversion was obtained from Station KBGR at the Bangor International Airport.

Tidal current velocity was obtained analytically for shallow and convergent estuaries following (Friedrichs, 2010). Tidal velocity amplitude (U_0) can be obtained by:

$$u_1 = \frac{\eta\omega L_w}{h}\frac{w_b}{w}$$ Eqn. 3.7 (Tidal Velocity Amplitude)

Where η is water surface elevation, ω is the angular frequency of the principal tide, L_w is the e-folding length based on width, h is the water column depth, and $\frac{w_b}{w}$ is a ratio of mean channel width (w_b) over a tidal cycle relative to channel width (w). This form includes the effect of convergence to approximate the velocity of tidal currents.

3.7 Results

The ice-free discharge of the Penobscot River cycles annually, with spring freshets in April and May spiking the Penobscot River to the yearly flow maxima (Fig. 13). Maximum and minimum discharges of the Penobscot River over the 7-year dataset were 2400 m^3/s and 50 m^3/s, respectively. The dry season of June, July, August, and September constituted the low flow period, where average discharge receded to 170 m^3/s. The 7-year average wind speed showed that the windier portion of the year (>4 m/s) in Downeast Maine is from November to May, spanning Fall, Winter, and early Spring (Fig. 13). Sustained wind speeds during storm events can produce winds greater than 10 m/s over this period.

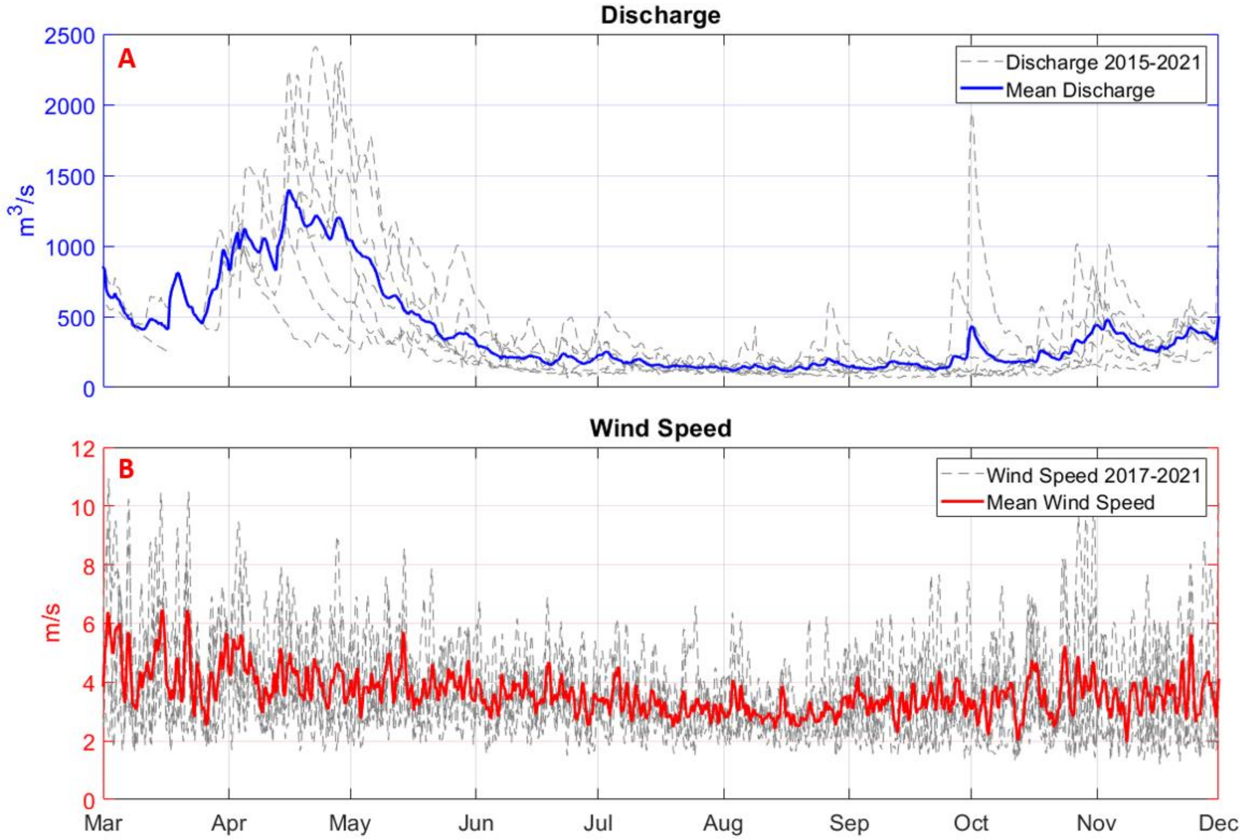

Figure 13: Environmental conditions proximate to the study site with (A) yearly discharge at West Enfield, ME in blue and (B) yearly wind speeds with a 5-year average in red. Single years are displayed in dashed gray.

3.8 Tidal Characterization

To understand the variation in tidal dynamics from the coast to the tidal river portion of the PRE, harmonic analyses over 7 years of water levels at Bar Harbor and Bangor were compared. At the coast, the tidal regime was predominately semidiurnal, indicated by a form factor of (K1+O1)/M2 = 0.16, which is < 0.25, the limit for semidiurnal regimes. The largest constituents were principal tides M2, N2, S2, and K1, with amplitudes of 1.57-m, 0.35-m, 0.24-m, and 0.14-m, respectively. Near the head in Bangor, the tides were still predominately semidiurnal, however, shallow water effects become important. The dominant harmonics are M2, N2, S2, and M6, with amplitudes of 1.67-m, 0.38-m, 0.26-m, and 0.17-m, respectively.

Power-frequency spectrums (Fig. 14) of water levels at Bangor, ME, calculated over a 7-year time series, indicated the semidiurnal tidal species to dominate fluctuations in water level. Overtides at four, six, eight, and ten cycles per day are also prominent, with the sixth-diurnal dominating the quarter-diurnal harmonic.

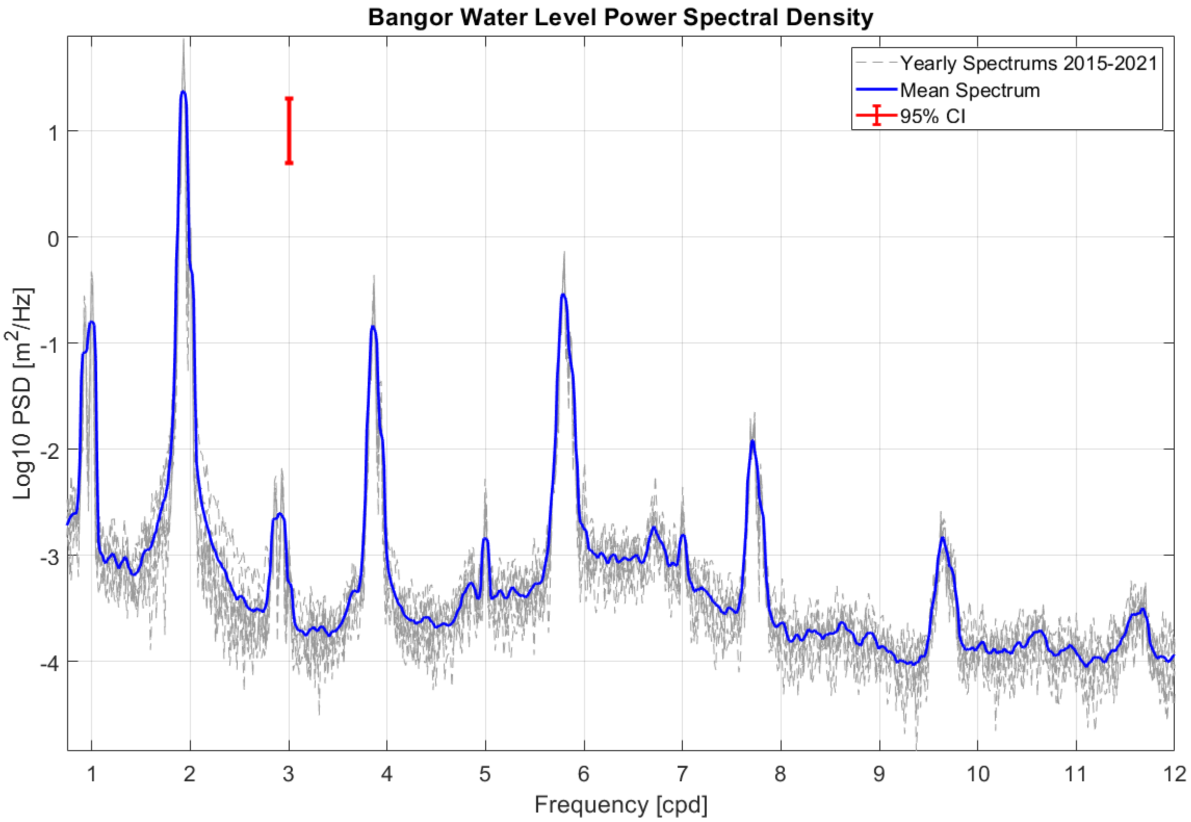

Figure 14: Power-frequency spectrums from water levels at Bangor USGS station 01037050. Yearly spectrums are plotted in light gray and a 7-year mean spectrum is highlighted overtop in blue. Peaks greater than the 95% confidence interval plotted in red are considered statistically significant.

3.9 Overtide & Mean Flow Relationship

Since the sixth-diurnal overtides tend to dominate the quarter-diurnal near the head of the PRE, it is important to look at how river discharge modulates the tidal harmonics. To explore this, a continuous wavelet transform was utilized to decompose and reconstruct frequency bands in time. Band amplitudes of the D2 tidal species vary in time as discharge and wind patterns vary seasonally, though this work will focus on river discharge. D2 amplitude increased during the summer months because the tide was unimpeded by large mean flows via river discharge (Fig. 15), known to dissipate the principal tide through the enhancement of effective bottom stress and transformation of energy to the D4 (Parker, 1984). D4 and D6 bands show an inverse relationship to each other with time, the D6 band grows to a maximum of 0.17 m during the low flow summer months while the D4 band decreases to 0.07 m minimum in August. D6 band amplitudes remain greater than D4 during the summer months as water column height lessens and mean flow decreases.

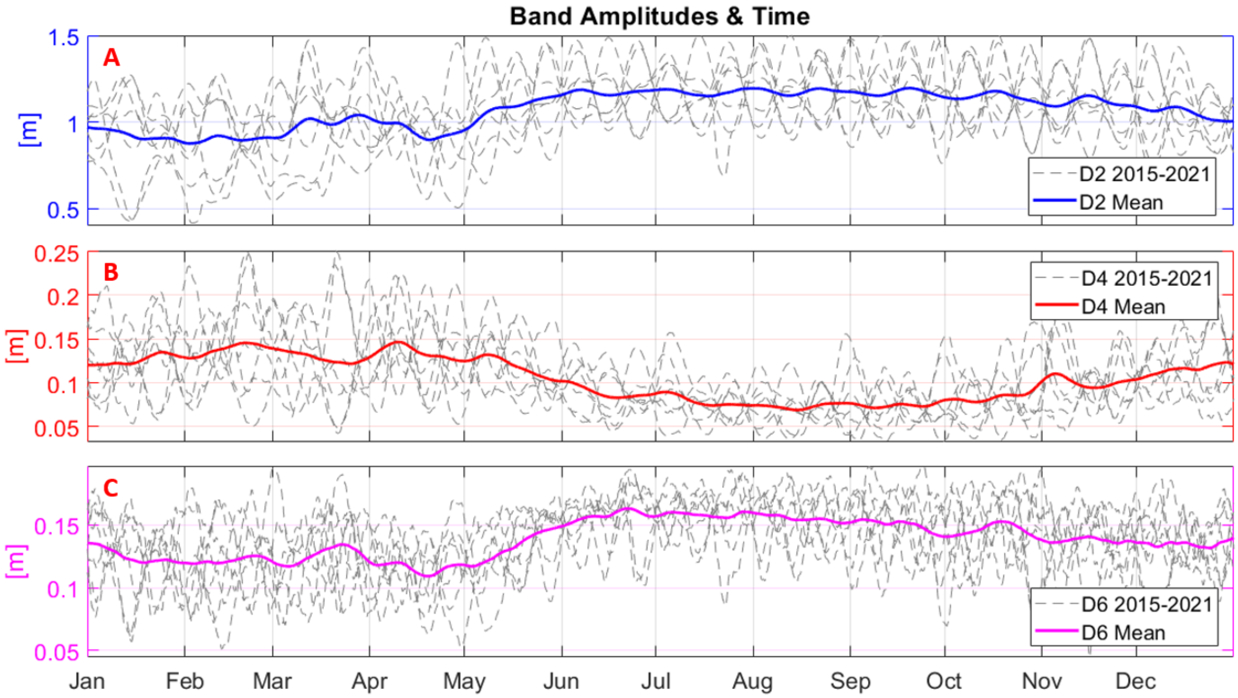

Figure 15: Band amplitude of the (A) D2, (B) D4, and (C) D6 tidal species at Bangor plotted in time. Thick, colored lines indicate the 7-year mean and grey dashed lines represent individual years.

The anticipated overtide patterns related to mean flow indicated a reduction in D6 during higher river discharge periods (higher mean flow), which coincided with larger asymmetric effects (D4). However, this representation includes the effect of river discharge and the spring-neap cycle modulating the principal tide. To isolate the influence of river discharge on overtides from how river discharge and spring-neap modulation affect the principal tide, the ratios of D4/D2 and D6/D2 were bin averaged (Fig. 16). Strength of asymmetry in the vertical tide is essentially the amplitude ratio of overtide to the principal (semidiurnal) constituent (Wong, 1991).

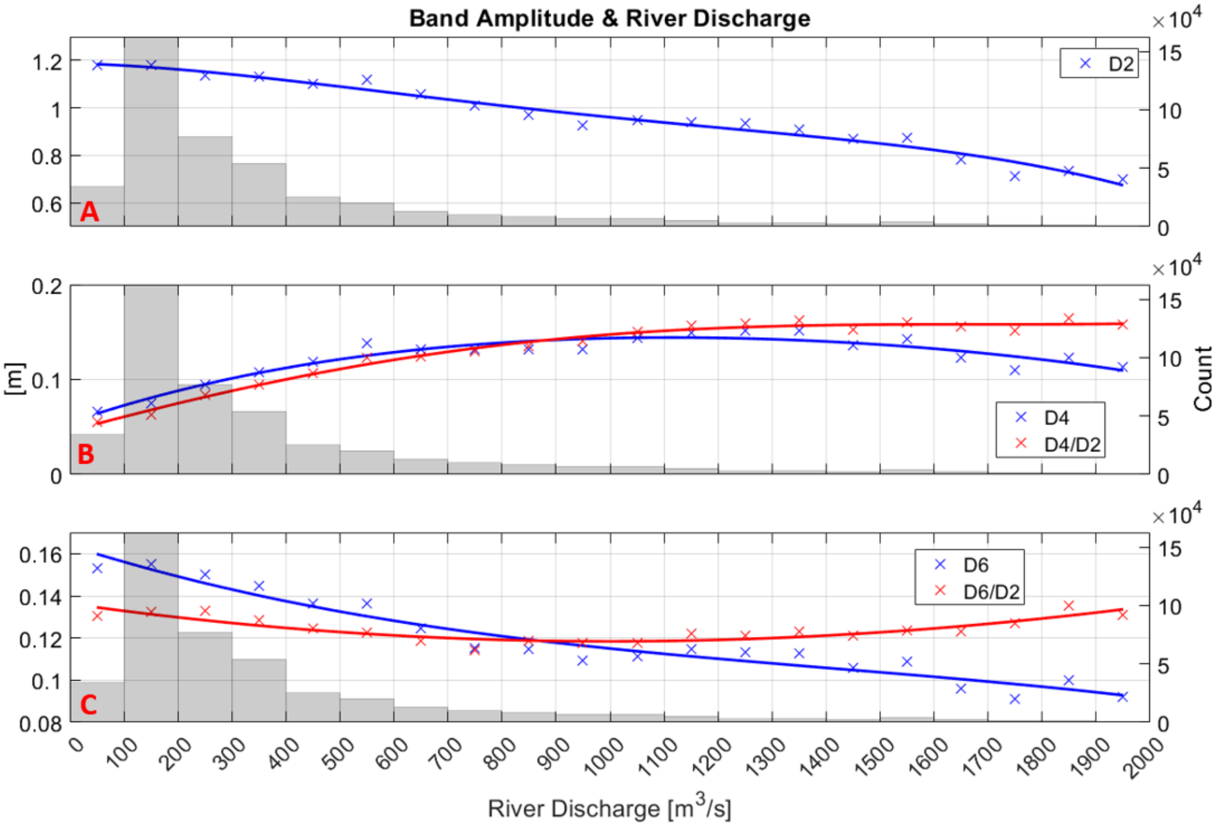

Figure 16: Band amplitudes of (A) D2, (B) D4, and (C) D6 designated in blue, and the D4 and D6 harmonics scaled by D2 are shown in red, binned by one hundred m^3/s river discharge increments. Bin averages designated by red and blue crosses possess fitted third-order polynomial curves included for highlighting trends. Histogram bin sizes shown in background gray correspond with the counts given on the right-orientated y-axis.

An inverse relationship of the D2 band amplitude was identified with increasing river discharge (Fig 16). This relationship was expected as a higher discharge coincides with a greater mean flow, and the interaction with the incident tide causes momentum loss from the main tidal constituent through the shallow water effects (Godin, 1999). D4 amplitude increased with increasing river discharge, as expected, since mean flows are known to enhance the asymmetric effects of energy transfer from the principal tide to D4 (Fig. 16) until a discharge of 1400-m^3/s. At higher discharges, the D4 remains constant with increasing discharge. The D4/D2 amplitude shows a similar pattern at river discharges smaller than 1400-m^3/s. Beyond this, D4/D2 decreases slightly, indicating a reduction in the asymmetric effect on the tides at high river discharges. While the D6 continuously decreased with increasing river discharge, the D6/D2 revealed an unexpected constant trend until 1400-m^3/s. Frictional generation of the D6 should continue while the mean flow is lesser than tidal velocity amplitude ($u_o<u_1$), as demonstrated in (Fig. 10). However, as this ratio approaches unity, the flow becomes unidirectional through the tidal cycle and quadratic friction's contribution to a third harmonic (D6) should cease. At discharges larger than 1400-m^3/s, an inverse relationship with D4 was observed, where D6/D2 increased. This trend is further elucidated through a binned relationship comparing the mean flow with tidal velocity amplitude, u_o/u_1 (Fig. 17). D2 amplitude decreases with increasing u_o/u_1, and the D6/D2 ratios at u_o/u_1 greater than one remain constant, deviating from Parker's theory presented in Fig. 10, necessitating an additional explanation for momentum transfer outside of quadratic friction.

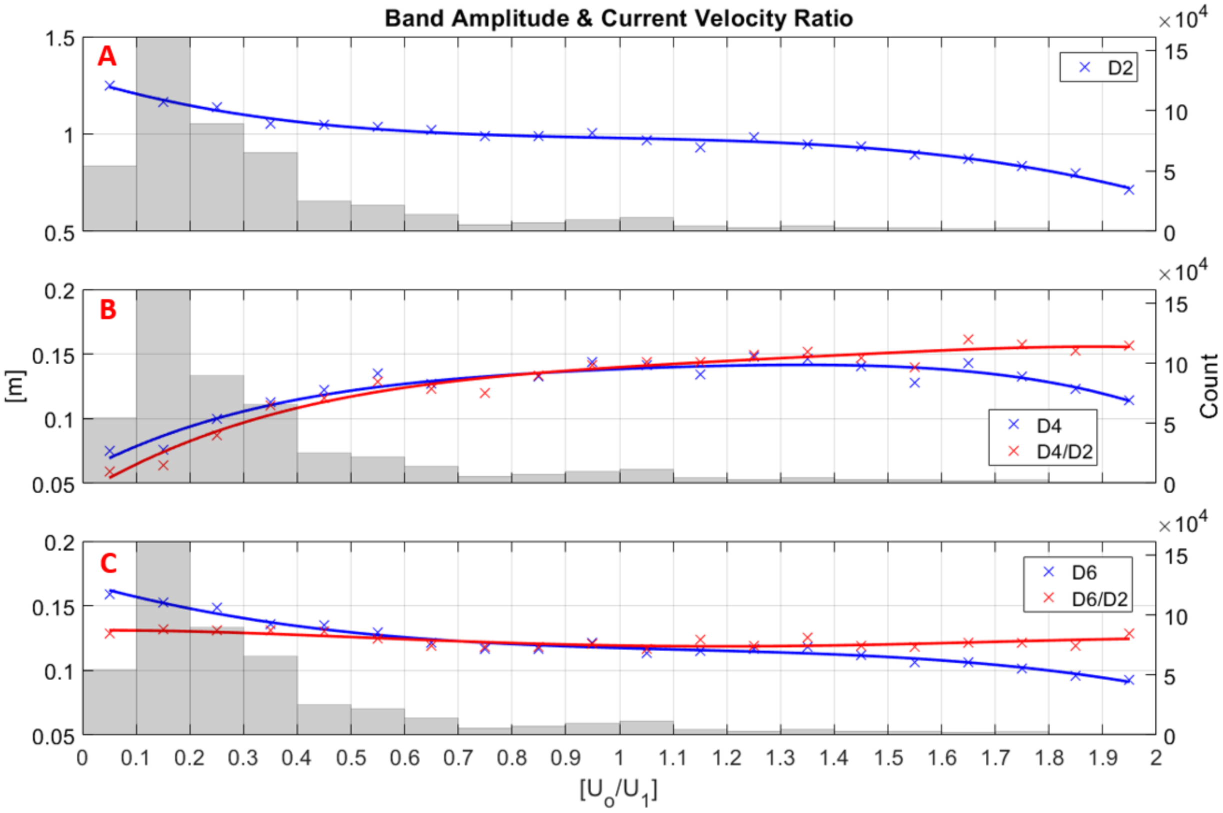

Figure 17: Band amplitudes of (A) D2, (B) D4, and (C) D6 designated in blue, and the D4 and D6 harmonics scaled by D2 are shown in red, binned by mean flow to tidal velocity amplitude ratio. Bin averages designated by red and blue crosses possess fitted third-order polynomial curves included for highlighting trends. Histogram bin sizes shown in background gray correspond with the counts given on the right-orientated y-axis.

3.10 In-Situ Observations

To understand why D6/D2 remains constant with increasing discharge rather than decreasing, an investigation into the momentum terms that form D4 and D6 is warranted. A tidal cycle survey was conducted during low (<200 m^3/s) river discharge conditions. To understand what mechanisms are contributing to the D4 and D6 overtides, the in-situ observations were used to calculate each of the forcing terms that lead to overtides (Fig. 18). *Quadratic friction* ($\frac{u|u|}{h_0}$) was the greatest momentum term by an order of magnitude, obtaining a maximum of $1 \, x \, 10^{-3}$ at the same time as *advection* ($u\frac{\partial u}{\partial x}$) $8.3 \, x \, 10^{-5}$, and *nonlinear continuity* ($\frac{\partial (u\eta)}{\partial x}$) $4.2 \, x \, 10^{-5}$ during peak flood currents, occurring from 9-10 AM. This result was found during relatively low river discharge conditions, where the importance of *quadratic friction* is expected due to the lower water depths and reduced mean (river) flows. The curve of *depth variation* $(\frac{\eta u|u|}{h_0^2})$ follows that of channel velocity until a deviation at the end of ebb, where the channel depth is low and the h_0^2 term in the denominator becomes small, increasing the value of *depth variation* to a maximum of $7.3\ x\ 10^{-4}$.

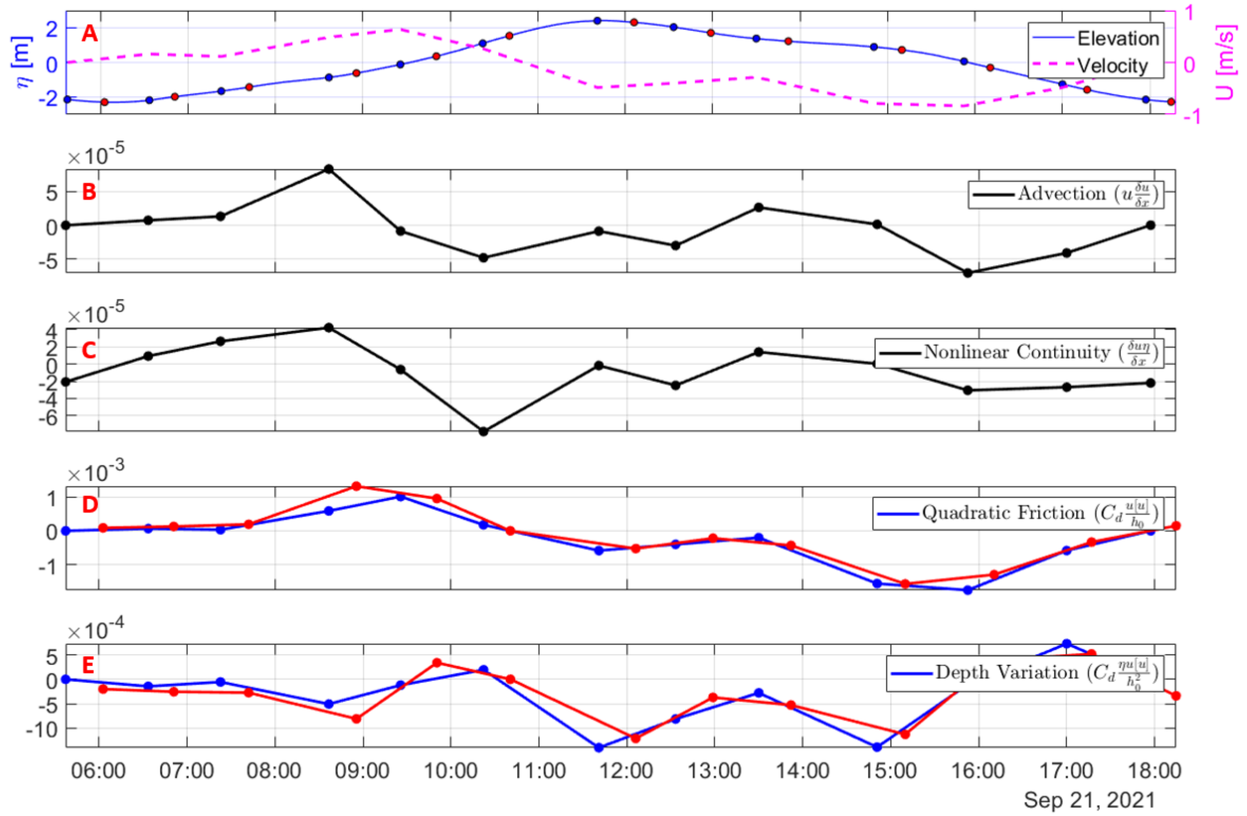

Figure 18: Water level and channel velocity (A) and nonlinear terms (B) *advection*, (C) *nonlinear continuity*, (D) *quadratic friction*, and (E) *depth variation* plotted in time. The dashed magenta line in (A) outlines the average channel velocity from both the North and South transect, plotted on the North transect sampling times. Blue and red-filled circles in (A) designate North and South transects, respectively. Filled circles and connecting lines in (D) & (E) designate nonlinear terms calculated with velocities from North (blue) and South (red) transects.

A harmonic analysis was conducted on the current velocities and water levels to understand the relationship between D2, D4 and D6 oscillations in context of periods with the greatest frictional influence (Figure 19). Elevated UD2 (>0.25 m/s) occurred from 7:00 – 9:00 EDT during flood and coincided with a modulation in the D6 from quadratic friction that resulted in an amplitude of UD6 = -0.22 m/s. This resulted in minimal tidal distortion, as the ηD2+D4+D6 (black line in Fig. 19A) was only slightly smaller than ηD2 (blue line). During ebb, elevated UD2 (> -0.25 m/s) occurred from 13:00 - 15:00 LST, which resulted in an amplitude of UD6 = 0.22 m/s. However, the distortion effect on the tide was more prominent, as seen by ηD2+D4+D6 that was smaller than ηD2. This is likely due to quadratic friction and depth variation being out of phase during flood, thereby deconstructively interfering and causing minimal distortion on ηD2. Conversely during ebb, quadratic friction and depth variation are in phase, leading to a larger modulation of ηD2. Reconstructed water levels illustrate that the pronounced tidal distortion on ebb on the day of sampling arises from D4 & D6 bands acting in concert, working in phase to create a delay in low water (Fig. 19). This is evident in the reconstructed current velocities at 2 PM, where the increasing reconstructed D6 band velocity lines up with the slowing of measured ebb velocity. The dashed line of measured current velocities exhibits similar curvature to the D2+D4+D6 reconstruction but slightly overestimates the velocities on flood and underestimates on ebb phase. This highlights the importance of the second and third harmonics of the semidiurnal tide, as reconstructions of these alone do well as a first-order approximation.

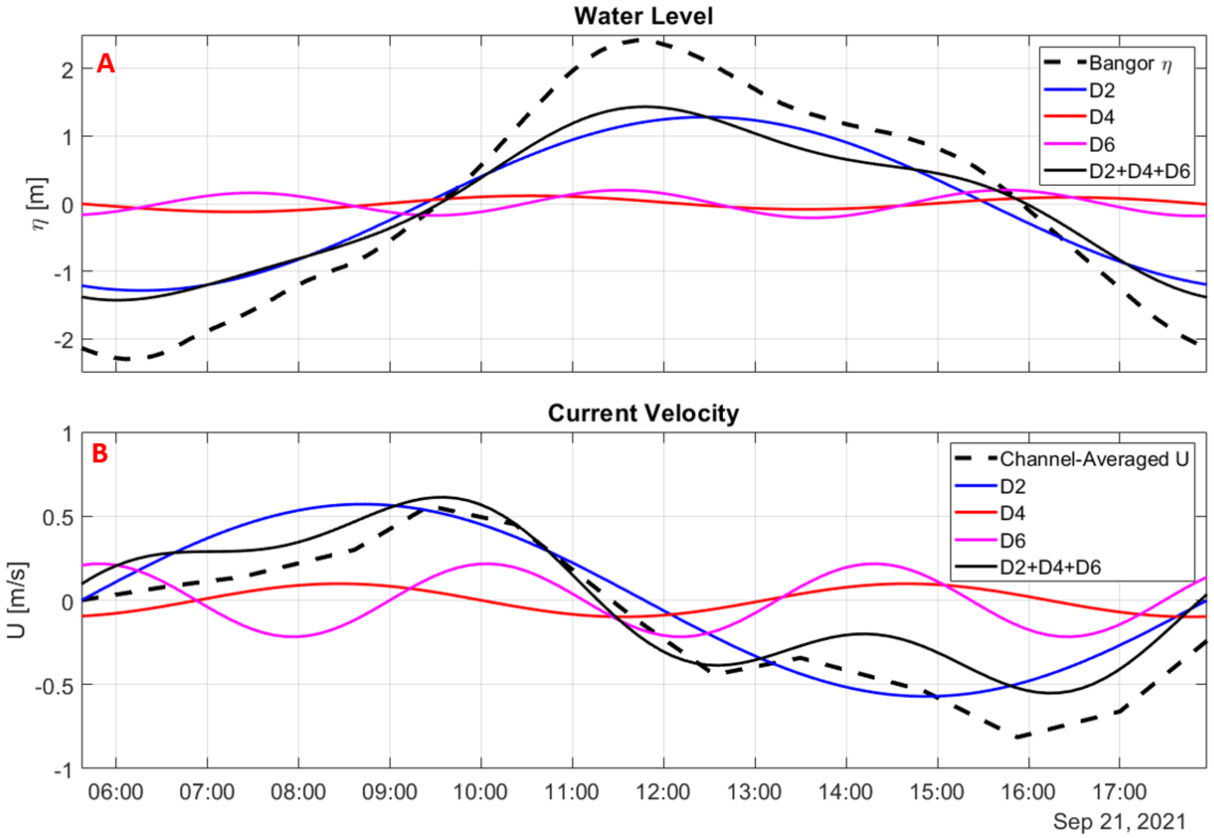

Figure 19: (A) Bangor water level on September 21st, 2021, from the Bangor USGS station displayed in dashed black with reconstructed water levels of D2 (blue), D4 (red), D6 (magenta), and their aggregate contribution (black) from wavelet analysis. (B) measured channel velocity (dashed black) and reconstructed bands velocities obtained for each band by a least-squares fit on the measured depth-average channel velocities.

3.11 Discussion

The observations reveal an unanticipated behavior for the D6 overtide, where D6/D2 amplitudes are unaffected by increasing mean flows. If D6 were solely generated by quadratic friction, as suggested by the in-situ observations, this trend is in violation of theory in a tidal river with significant mean flows. In this discussion the potential for another mechanism to enhance the D6 is explored. Momentum transfer to a third harmonic due to tidal reflection off abyssal ridges is a possible explanation and has been identified in Valle-Levinson et al. (2007). While studying depth-dependent overtides, Valle-Levinson et al. (2007) found that internal tides reflected at abrupt bathymetry such as a sill in a glacial fjord interacted with incident barotropic tides to create distortions linked to sixth-diurnal oscillations in the vertical and horizontal tide. Next, an investigation explores if this dynamic holds for barotropic tides reflecting off hardened structures (such as a partially removed dam) in tidal rivers, thereby creating a reflected wave that interacts with the incident to produce sixth-diurnal oscillations. Theoretical results produce sixth-diurnal oscillations through the nonlinear interaction of the incident principal tide, and its reflected self, mathematically described by $[sin(\sigma D_2 t)\ \times\ |sin(\sigma D_2 t)|]$ (Parker, 1991; Valle-Levinson et. al, 2007). Some portion of the D6 fluctuations observed in water levels at Bangor may then be a synthetic result that is unaffected by river discharge. Partial tidal reflection off a decommissioned, but not fully removed dam at Veazie, ME, 2.5km upstream of the USGS station at Bangor, may offer an explanation for the elevated sixth-diurnal oscillations found at Bangor. The Veazie hydroelectric dam was the most seaward obstruction on the Penobscot River before it was removed in the summer of 2013. To demonstrate this, a conceptual analysis that shows the nonlinear interaction of a reflected tide with itself can create a D6 harmonic, and that the amplitude of the D6 harmonic generated is independent of the amplitude of the reflected wave (Fig. 20). It is also important to illustrate that the tidal waveform at Bangor expresses distortion remarkably similar to the superposition of solely D2 and D6 components, through the full range of phase lags (0-2π).

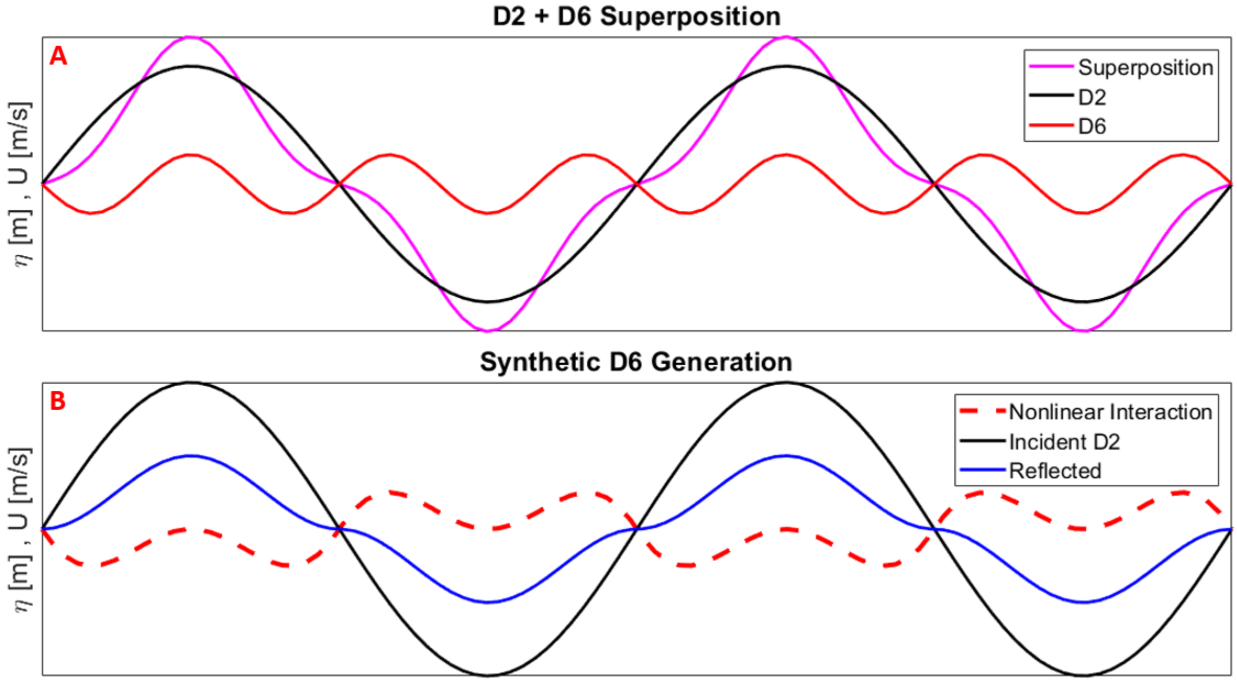

Figure 20: Conceptual relationships of (A) D2, D6, and their superposition over two semidiurnal tidal cycles highlighting the distortion caused by solely the addition of D2 and a D6 with a phase lag of π, and (B) the relationship of an incident and partially reflected D2 wave and the emergence of a sixth-diurnal harmonic.

To further demonstrate that the enhanced D6 harmonic over the D4, and its disconnection to river discharge may be influenced by the nonlinear interaction between the principal tide reflecting off the partial dam, a HOBO pressure sensor was deployed upstream of the Veazie dam site. During the period of deployment, the average discharge of the Penobscot River was 384 m^3/s, which is greater than the dataset average. Water level spectra on either side of the dam can be compared to see if the dam is creating a larger D6 signal through partial reflection compared to the D4. If the dam is enhancing the D6, it is expected that the D4 would dominate D6 on the landward side of the dam (Fig. 21).

Seaward of the dam, at Bangor, the D6 band dominates D4, while at the HOBO pressure sensor location upstream of the obstruction, this trend reverses. In addition to this, a decrease in spectral power attributed to the D2 band indicates partial reflection due to the dam site. The reduction in total amplitude in the tide between Bangor and the HOBO pressure sensor location, separated by 3.5 km, can be quantified by a transmission coefficient (Kt) of 0.46. Representing an average ratio of the total amplitude of the transmitted wave relative to the incident wave for the HOBO deployment, November 10th-29th 2021. This attenuation recognized in the principal tide is likely due to a combination of tidal reflection and back water effects, which are known to attenuate the tide by the addition of a gradient to water level.

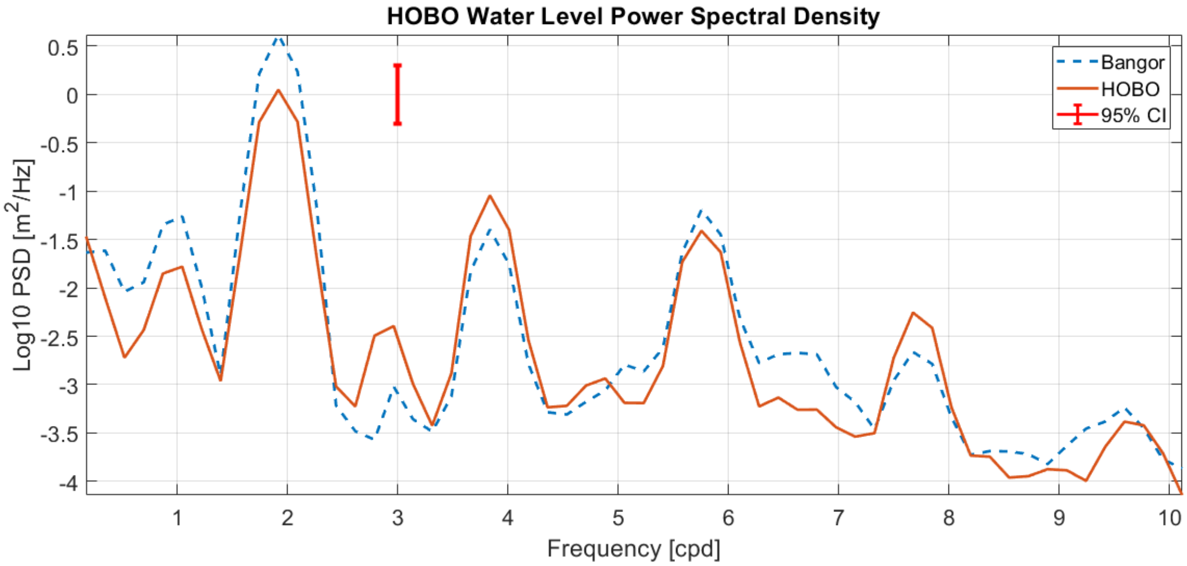

Figure 21: Water level power-frequency spectrums of Bangor and HOBO pressure sensor location water levels over November 10th-29th 2021. Peaks greater than the 95% confidence interval plotted in red are considered statistically significant.

This finding suggests that partial tidal reflection owed to anthropogenic structures hindering the propagation of tides is a mechanism that can enhance the amplitudes of overtides in estuaries. This has implications for longitudinal variation in tidal dynamics for tidal waves propagating along a fluvial-marine transition, as tidal dynamics downriver of channel obstructions may differ from those beyond.

Limitations of this study include the lack of observations upstream of the dam to evaluate tidal reflection more thoroughly. Water level and velocity sensors placed before and after the dam could allow the separation of incident and reflected waves. Further work is also necessary to resolve the spatial variability of overtide generation in estuaries, with a particular emphasis on tidal river reaches. Additional studies would do well to involve a validated 3d model to resolve spatial scales not captured in this observational work.

3.12 Conclusion

The goal of this research contribution was to investigate the mechanisms generating an amplified D6 band at the landward extents of tidal rivers. We demonstrated the emergence of tidal reflection as a key mechanism in the generation of a third harmonic even under conditions of high discharge. This study has also shown the importance of including both contributions of external tidal and fluvial forcing to improve tide predictions in the landward regions of tidal rivers. This work is important as common studies of tide-river interaction are conducted in stable rivers or rivers with limited variability in river discharge, limiting the variability of tide-river interaction, and leaving the effects of river discharge on tides poorly understood.

CHAPTER 4

CONCLUSION

The goal of this research contribution was to investigate the mechanisms modulating tidal asymmetry and overtide generation proximate to the study site in the Penobscot River Estuary. The goal was accomplished through the analysis of long-term water level and discharge records in the Penobscot River, and in-situ field observations collected in the river. The findings of this thesis offer insight into the mechanisms that control the water level and currents in tidal rivers, at the landward extents of estuaries. Preceding work in this vein of river-tide interaction has focused on the effect of mean flow on tidal propagation for implications in tidal range, vertical current structure, and spatial dissipation (Friedrichs, 2010; Cai et al., 2014; Elahi et al., 2020; Dykstra et al., 2022). Additionally, studies sought to relate river discharge to sediment transport in highly nonlinear systems, backwater profiles in rivers with sloping beds, and parametrization of bulk friction terms for increased ebb-cycle discharges (Fry, 1981; Yoon, 2013; Kastner, 2019). We demonstrated the emergence of partial tidal reflection as a mechanism important in the generation of a sixth-diurnal harmonic born from nonlinear interaction between the incident and reflected waves. Nonlinear interactions between tidal components are essential in studies of sediment transport because they instigate asymmetries of flow velocity, sediment flux, erosion, and deposition.

This contribution has focused primarily on overtide generation with implications in asymmetry in the vertical tide (water level), however, asymmetry in the horizontal tide (currents) is equally important because of its relation to morphological development via residual sediment transport (Wang et al. 1999). Additional studies would do well to focus on tidal current velocities and span a long enough period to capture large variability in river discharge.

New and advanced non-stationary harmonic analysis techniques such as the NS_Tide toolbox (Matte et al. 2012) are improving the way researchers can study these nonstationary signals, allowing the reconstruction of time series into subtidal and tidal properties. Further studies applying such techniques will allow the identification of modulations of the tide caused by nontidal processes that still manifest in tidal frequency bands.

REFERENCES

Amirbahman, A., & Merritt, K. A. (2008). Mercury in the Penobscot River Estuary: The Sediment-Water Interface. *Marine Research in Focus*, *5*, 1–4. w.seagrant.umaine.edu/files/pdf-global/08RIFHg.pdf

Bears, K. (2018). *The Dynamics of Mixing and Subtidal Flow in a Maine Estuary*.

Burchard, H., Hetland, R. D., Schulz, E., & Schuttelaars, H. M. (2011). Drivers of residual estuarine circulation in tidally energetic estuaries: Straight and irrotational channels with parabolic cross section. *Journal of Physical Oceanography*, *41*(3), 548–570. https://doi.org/10.1175/2010JPO4453.1

Burchard, H., & Rennau, H. (2008). Comparative quantification of physically and numerically induced mixing in ocean models. *Ocean Modelling*, *20*(3), 293–311. https://doi.org/10.1016/j.ocemod.2007.10.003

Case, J. (1999). Understanding Tides — From Ancient Beliefs to Present-day Solutions to the Laplace Equations. *SIAM News*, *33*(2), 1–4.

Dias, J. M., Valentim, J. M., & Sousa, M. C. (2013). A numerical study of local variations in tidal regime of Tagus estuary, Portugal. *PLoS ONE*, *8*(12). https://doi.org/10.1371/journal.pone.0080450

Friedrichs, C. T., & Aubrey, D. G. (1988). Non-linear tidal distortion in shallow well-mixed estuaries: a synthesis. *Estuarine, Coastal and Shelf Science*, *27*(5), 521–545. https://doi.org/10.1016/0272-7714(88)90082-0

Fry, V. A. (1987). Tidal velocity asymmetries and bedload transport in shallow embayments. *Tidal Velocity Asymmetries and Bedload Transport in Shallow Embayments*. https://doi.org/10.1575/1912/4801

Georgas, N. (2012). Large seasonal modulation of tides due to ice cover friction in a large midlatitude estuary. *Journal of Physical Oceanography*, 42(3), pp.352-369

Geyer, W. R., & MacCready, P. (2014). The estuarine circulation. *Annual Review of Fluid Mechanics*, *46*(August 2013), 175–197. https://doi.org/10.1146/annurev-fluid-010313-141302

Godin, G. (1995). Rapid evolution of the tide in the Bay of Fundy. *Continental Shelf Research*, *15*(2–3), 369–372. https://doi.org/10.1016/0278-4343(93)E0005-S

Great Works & Veazie Dams Removed from Penobscot River. Natural Resources Council of Maine. (2013). https://www.nrcm.org/programs/waters/penobscot-river-restoration-project/great-works-dam-veazie-dam-removal/

Guo, L., Zhu, C., Cai, H., Wang, Z. B., Townend, I., & He, Q. (2021). River-enhanced non-linear overtide variations in river estuaries. *Hydrology and Earth System Sciences Discussions*, *February* 1–31. https://doi.org/10.5194/hess-2021-75

Hansen, D. V. (1966). *OCEANOGRAPHY*. *July*.

Hodgkins, G. A. (1999). Estimating the Magnitude of Peak Flows for Streams in Maine for Selected Recurrence Intervals: U.S. Geological Survey Water-Resources Investigations Report 99-4008, 45 p.

Kästner, K., Hoitink, A. J. F., Torfs, P. J. J. F., Deleersnijder, E., & Ningsih, N. S. (2019). Propagation of tides along a river with a sloping bed. *Journal of Fluid Mechanics*, *August*, 39–73. https://doi.org/10.1017/jfm.2019.331

Kowalik, Z., & Luick, J. L. (2019). Modern theory and practice of tide analysis and tidal power. *Austides Consulting*, 1–220.

Lieberthal, B., Huguenard, K., Ross, L., & Bears, K. (2019). The Generation of Overtides in Flow Around a Headland in a Low Inflow Estuary. *Journal of Geophysical Research: Oceans*, *124*(2), 955–980. https://doi.org/10.1029/2018JC014039

Lieberthal, B., Huguenard, K., Ross, L., & Liu, Z. (2019). Intratidal variability of water quality in the Damariscotta River, Maine. *Water (Switzerland)*, *11*(12). https://doi.org/10.3390/w11122603

Lueck, R. G., Wolk, F., & Yamazaki, H. (2002). Oceanic velocity microstructure measurements in the 20th century. *Journal of Oceanography*, *58*(1), 153–174. https://doi.org/10.1023/A:1015837020019

Nascimento, F. P. S., Valle-Levinson, A., Sottolichio, A., & Senechal, N. (2019). Overtide generation by wind-induced waves in a tidal inlet of SW France. *Continental Shelf Research*, *174*(March 2018), 66–75. https://doi.org/10.1016/j.csr.2019.01.007

Parker B.B., 1984. Frictional effects on tidal dynamics of shallow estuary. PhD. Dissertation, The Johns Hopkins University, 291 pp.

Parker B.B., 1991. The relative importance of the various nonlinear mechanisms in a wide range of tidal interactions. In: B.B. Parker (ed.), Tidal Hydrodynamics, John Wiley, New York, pp.237–268.

Ralston, D. K., & Geyer, W. R. (2019). Response to Channel Deepening of the Salinity Intrusion, Estuarine Circulation, and Stratification in an Urbanized Estuary. *Journal of Geophysical Research: Oceans*, *124*(7), 4784–4802. https://doi.org/10.1029/2019JC015006

Rockwell Geyer, W., & Ralston, D. K. (2018). A mobile pool of contaminated sediment in the Penobscot Estuary, Maine, USA. *Science of the Total Environment, 612,* 694–707. https://doi.org/10.1016/j.scitotenv.2017.07.195

Spicer, P. (2019). Tide and Storm Surge Dynamics in Estuaries of Variable Morphology. *Master Thesis.*, *January*. https://digitalcommons.library.umaine.edu/etd/2993

Spicer, P., Matte, P., Huguenard, K., & Rickard, L. (2021). Coastal windstorms create unsteady, unpredictable storm surges in a fluvial Maine estuary. *Shore & Beach*, *89*(2), 3–10. https://doi.org/10.34237/1008921

Torrence, C., & Compo, G. P. (1998). A Practical Guide to Wavelet Analysis. *Bulletin of the American Meteorological Society*, *79*(1), 61–78. https://doi.org/10.1175/1520-0477(1998)079<0061:APGTWA>2.0.CO;2

Valle-Levinson, A. (2021). Dynamics-based classification of semienclosed basins. *Regional Studies in Marine Science*, *46*, 101866. https://doi.org/10.1016/j.rsma.2021.101866

Valle-Levinson, A., Reyes, C., & Sanay, R. (2003). Effects of bathymetry, friction, and rotation on estuary-ocean exchange. *Journal of Physical Oceanography, 33*(11), 2375–2393. https://doi.org/10.1175/1520-0485(2003)033<2375:EOBFAR>2.0.CO;2

Valle-levinson, A. A., Blanco, J. L., Frangópulos, M., Valle-levinson, A., Blanco, J. L., Frangopulos, M., Engineering, C., & Hall, W. (2020). Depth-dependent Overtides from Internal Tide Reflection in a Glacial Fjord Linked references are available on JSTOR for this article: Depth-dependent Overtides from Internal Tide Reflection in a Glacial Fjord. *Estuaries and Coasts*, *30*(1), 127–136.

Matte, P., Jay, D. A., & Zaron, E. D. (2013). Adaptation of classical tidal harmonic analysis to nonstationary tides, with application to river tides. *Journal of Atmospheric and Oceanic Technology*, *30*(3), 569–589. https://doi.org/10.1175/JTECH-D-12-00016.1

Wang Z.B., Juken H., de Vriend H.J., 1999. Tidal asymmetry and residual sediment transport in estuaries. WL|Hydraulic, report No. Z2749, 66 pp.

Whitfield, A., & Elliott, M. (2012). Ecosystem and Biotic Classifications of Estuaries and Coasts. In *Treatise on Estuarine and Coastal Science* (Vol. 1, Issue March 2018). Elsevier Inc. https://doi.org/10.1016/B978-0-12-374711-2.00108-X

Wu, Y., Hannah, C., Matte, P., O'Flaherty-Sproul, M., Mo, R., Wang, X., & MacAulay, P. (2022). Tidal propagation in the Lower Fraser River, British Columbia, Canada. *Estuarine, Coastal and Shelf Science*, *264*(November 2021), 107695. https://doi.org/10.1016/j.ecss.2021.107695

Yoon, B., & Woo, S.-B. (2013). Tidal asymmetry and flood/ebb dominance around the Yeomha channel in the Han River Estuary, South Korea. *Journal of Coastal Research*, *165*, 1242–1246. https://doi.org/10.2112/si65-210.1

Zhu, L., He, Q., & Shen, J. (2020). Response of Stratification Processes to Tidal Current Alteration due to Channel Narrowing and Deepening. *Journal of Geophysical Research:*

UMAINE MOU. (2018). *Memorandum of Understanding Between the Penobscot Nation and the University of Maine System, University of Maine (Orono)*. https://umaine.edu/nativeamericanprograms/wp-content/uploads/sites/320/2018/05/Penobscot-Nation-UMaine-MOU.pdf

BIOGRAPHY OF THE AUTHOR

Matt Fischer was born in Anchorage, Alaska on the morning of July 20th, 1995. He is a proud graduate of East Anchorage High School and the University of Alaska, Anchorage. Matt is a candidate for the Master of Science degree in Civil and Environmental Engineering from The University of Maine in December 2022.